The ocean-driven instability of the South Pacific sector of the West Antarctic Ice Sheet since 773 ka

Jiakai Wang[1,3], Zheng Tang[2,4], Fengming Chang[1,3,4], Qingyun Nan[1,3,4], Zhifang Xiong[2,4], Tiegang Li[2,3,4*]

[1] Key Laboratory of Marine Geology and Environment, Institute of Oceanology, Chinese Academy of Sciences, Qingdao 266071, China;

[2] Key Laboratory of Marine Geology and Metallogeny, First Institute of Oceanography, Ministry of Natural and Resources, Qingdao 266061, China;

[3] University of Chinese Academy of Sciences, Beijing, 100049;

[4] Laboratory for Marine Geology, Qingdao National Laboratory for Marine Science and Technology, Qingdao 266237, China

*Corresponding author: T. G. Li (tgli@fio.org.cn)

Key Points:

- Ocean-driven positive feedback significantly influences the vulnerability of the West Antarctic Ice Sheet since 773 ka.
- The variations in sediment provenance indicate the changes in iceberg trajectory, which relate to the shift in atmospheric circulation.
- We suggest that the West Antarctic Ice Sheet variation is sensitive to the local summer insolation forcing since 773 ka.

Abstract: Insight into the causes of the West Antarctic Ice Sheet (WAIS) stability over middle Pleistocene glacial/interglacial (G/IG) cycles is fundamental to our understanding of the response of the climate system to the cryosphere. Here, to clarify the mechanism of WAIS stability during the late Quaternary period, we provide iceberg-rafted debris (IRD) contents, clay mineral, and Sr-Nd isotopic analyses of the piston core ANT34/A2-10. The core was recovered from the seasonal sea ice region in the Antarctic Zone of the Amundsen Sea with a ~773 ka BP chronology. The endmember analysis of clay minerals shows marked differences in sediment provenance at site ANT34/A2-10 between IRD peak interval and low IRD content

interval in G/IG cycles. And the Sr-Nd isotopic endmember analysis in IRD peak intervals restricts the sediment provenance in the Victoria Land. We suggest that shifts in the sediment provenance resulted from the variations in iceberg trajectories, which connected to the significant shifts in the atmospheric system at the IRD peak intervals. Moreover, a contemporaneous strengthened ocean-driven positive feedback occurred between the increased wind-driven upwelling of warm, well-ventilated Circumpolar Deep Water and the intense ice mass loss process (including iceberg calving and basal melting process) with the instability of the WAIS. Furthermore, our results reveal that the variation of WAIS stability is sensitive to the local summer insolation forcing. These pieces of evidence recorded in the pelagic South Pacific Southern Ocean may strongly reflect the significant variations in ocean-driven and orbital forcing on WAIS stability on the orbital scale.

Keywords: WAIS stability, ocean-driven positive feedback, iceberg-rafted debris, clay mineral, Sr-Nd isotopes

Plain Language Summary

The vulnerability of the West Antarctic Ice Sheet (WAIS) has a significant influence on accelerating the global sea-level rise in recent decades. Previous studies have pronounced that the oceanic-driven feedback process could exert significant control on accelerating the iceberg calving and ice shelf basal melting process in the Amundsen sector of WAIS. Meanwhile, this process could also lead to the grounding line retreat, causing the buttress loss of the glacier and fast ice stream in this sector. Previous studies focus on clarifying this feedback process in the recent glacial/interglacial cycle. However, the evidence of this feedback is rare to find in the long-term orbital scale study in the south pacific Southern Ocean. For this purpose, we provide long-term Iceberg-Rafted Detritus (IRD), clay mineral, and Sr-Nd isotopic records, combined with the gradient of benthic $\delta^{13}C$ between intermediate South Atlantic Ocean to deep South Pacific Ocean and EDC ice core records to prove the existence of ocean-driven positive feedback process since 773 ka. The endmember

analysis of clay minerals and Sr-Nd isotopic composition in high IRD content periods could indicate the iceberg trajectory variation due to the shift of the atmospheric circulation that consists with the ocean-driven feedback.

1 Introduction

Ice sheet stability plays an essential role in the global climate system by influencing the sea level, oceanic circulation, and global carbon cycle at different time scales (Wadham et al., 2019, Golledge et al., 2019, Lear et al., 2004, Lindgren et al., 2018, Bell, 2008). In particular, the Antarctic Ice Sheet will be the largest contributor reservoir for potential global sea level rise (Tinto et al., 2019, Nerem et al., 2018, team, 2018). Recent studies indicate that the Antarctic Ice Sheet mass loss contribution to sea level rise has considerably increased in recent years, primarily related to iceberg calving and basal melting processes (Rignot et al., 2019, Shepherd et al., 2018). The current ice mass loss of the Antarctic ice sheet is concentrated in the West Antarctic Ice Sheet (WAIS), where the basal melting of floating ice shelves are accelerating the retreat of the 'grounding line' (the junction of ice, ocean, and bedrock) (Pattyn and Morlighem, 2020). This contemporary process also exists in different time scales and was proved by model simulation (Larour et al., 2019, Pritchard et al., 2012, Joughin and Alley, 2011, Pollard and DeConto, 2009) and geological investigation (Levy et al., 2019, Conway et al., 1999).

The South Pacific Sector (SPS) of WAIS is mainly located adjacent to the Ross Sea (RSE) and Amundsen Sea (ASE) embayments, including the Ross Ice Shelf, Thwaites Glacier (TG), Getz Ice Shelf (GIS), and Pine Island Ice Shelf (PIIS), and these ice shelf buttresses the rapidly flowing inland ice streams from the SPS of the WAIS, preventing their drainage into the Southern Ocean (Joughin and Alley, 2011, Pritchard et al., 2012, Davis et al., 2018) (fig. 1). Studies suggest that the grounding line beneath this sector of the WAIS is retreating irreversibly southward due to ocean-driven ice mass loss and may cause the buttresses loss of floating ice shelf and accelerate the further ice mass loss of this sector of WAIS (Lowe and Anderson, 2002, Turney et al., 2020, Rignot et al., 2013, Schmidtko et al., 2014, Rignot et al., 2019,

Rignot et al., 2014, Thoma et al., 2008, Jacobs et al., 2011, Joughin et al., 2014, Jones et al., 2021). The ice mass loss mainly involves iceberg calving and basal melting in SPS of the WAIS, accounting for the dominant total ice mass loss in the glacier and ice shelves of this sector (team, 2018). In the traditional view, ablation from the Antarctic Ice Sheet primarily originates from the iceberg calving process, with basal melting contributing approximately 20% of the total Antarctic Ice Sheet mass loss (Jacobs et al., 2017). In recent decades, estimations suggest that the iceberg calving from the entire Antarctic Ice Sheet accounts for up to 1389 Gt yr^{-1}, representing half of the total Antarctic Ice Sheet mass loss (Gladstone et al., 2001, Silva et al., 2006).

However, investigations show that the increasing upwelling of relatively warm Circumpolar Deep Water (CDW) and/or Modified Circumpolar Deep Water (MCDW) in the South Pacific Southern Ocean has accelerated the basal melt rate in the SPS of the WAIS (Jacobs et al., 1996, Rignot et al., 2013, Jacobs et al., 2011, Thoma et al., 2008, Gladstone et al., 2001). This phenomenon suggests that the basal melting process is the primary cause of the present ice mass loss in the Amundsen and Bellingshausen seas (Pritchard et al., 2012, Thoma et al., 2008, Jacobs et al., 2011, Nakayama et al., 2018, Rignot and Jacobs, 2002). These ice discharge processes are useful to reveal the feedback between poleward wind-driven transport of warm CDW and subsurface warming of the Southern Ocean, and the destabilization of the WAIS is not only occurring in the present (Rignot et al., 2019, Shepherd et al., 2018) but has also occurred in recent glacial/interglacial (G/IG) cycles (Lowe and Anderson, 2002, Turney et al., 2020, Weber et al., 2014, Jones et al., 2021). However, very little is known about this ocean-driven feedback mechanism over long-term orbital time scales (Pollard and DeConto, 2009, Teitler et al., 2010, Levy et al., 2019).

Thus, to clarify the connection between WAIS stability and this ocean-driven process with the high-latitude atmospheric process variation on the orbital scale, we used the iceberg-rafted debris (IRD) content in core ANT34/A2-10, with benthic $\delta^{13}C$ gradient of the intermediate south Atlantic (ODP site 1088) to deep east equatorial Pacific (ODP site 849) and EPICA-Dome C (EDC) ice core data (accumulation rate in ice

equivalent per year) to trace the iceberg calving process of the WAIS (Weber et al., 2012, Kanfoush et al., 2000, Nielsen et al., 2007), with CDW ventilation (Hodell et al., 2003, Ullermann et al., 2016, Hodell and Venz-Curtis, 2006, Hall et al., 2001) and wind-driven upwelling of deep water (Members, 2013, Anderson et al., 2009) in the South Pacific Southern Ocean on the orbital scale, respectively. Furthermore, we combined the records of clay minerals and EDC accumulation rate to illustrate the overall differences of sediment provenances at site ANT34/A2-10 during G/IG cycles. Moreover, combine these records with Sr-Nd isotopic composition in the IRD peak interval to illustrate the relationship between high-latitude atmospheric circulation changes and the provenance at IRD peak interval on the orbital scale in the South Pacific Southern Ocean.

2 Regional setting

Core ANT34/A2-10, which is 4.54 m long and located at 125°35’31”W, 67°02’10”S, with a water depth of 4216.6 m, was drilled by *R/V* Xuelong in the 34th Chinese National Antarctic Research Expedition in water. The core site is located in the sea ice region in the Antarctic Zone at the northern edge of the Amundsen Sea and south of the SACCF (fig. 1). The Ross Sea and the Amundsen Sea lie between the South Antarctic Circumpolar Current Front (SACCF) and Marie Byrd Land with the Ross Ice Shelf (fig. 1a). The major water masses in the area of our study are the Antarctic Surface Water (AASW), MCDW, CDW, and Antarctic Bottom Water (AABW) (fig. 1). The AASW is the low-temperature (near freezing point) and low-salinity (between 34.1 and 34.5 psu) surface water (Jacobs, 1985). The AASW flows westward along the edge of the ice shelf, adjacent to the Amundsen Sea and the Ross Sea, then moves northward along the coast of Victoria Land, and finally joins the Antarctic Circumpolar Current (ACC) (fig. 1). The ACC is an important dynamic feature in this area and moves eastward around Antarctica and interacts with water masses along its path, carrying the warm, high-salinity CDW (Jacobs and Comiso, 1997, Jacobs et al., 2012, Budillon and Spezie, 2004). The modification of the incoming CDW product MCDW at the outer edge of the Ross Sea, which is a warmer (temperatures up to

0.3°C) and fresher water mass than the surrounding waters, is the primary source of heat, salt, and nutrients to the Ross Sea continental shelf region (fig. 1b) (Budillon and Spezie, 2004, Smith et al., 2006, Hiscock, 2004). The upwelling of CDW and MCDW takes place at the continental slope, locally protruding far onto the inner continental shelf under the WAIS in ASE and RSE, respectively (Jacobs et al., 2012, Das et al., 2020). Furthermore, cause intense basal melting of the Ross Ice Shelf, with PIIS and GIS and intense iceberg calving from these ice shelf fronts and Pine Island Glacier (PIG) and TG in the RSE and ASE, respectively (fig. 1) (Jacobs et al., 1996, Walker et al., 2007, Thoma et al., 2008, Rignot and Jacobs, 2002, Jacobs et al., 2012), causing the recent ice mass loss of WAIS (Das et al., 2020, Adusumilli et al., 2020). Hence, the South Pacific sector of marine-based WAIS is considered one of the most instable regions in response to modern ocean heat flux changes.

3 Materials and methods

Core ANT34/A2-10 was split lengthwise and logged in detail by visual examination. Its lithology is characterized by continuous terrigenous deposition, mainly pelagic nannofossil clay, except for a foraminifer-rich layer at 11-29 cm and a radiolarian-rich layer at 0-90 cm. No evidence of turbidite sedimentation, bioturbation, or mass redeposition was found during the sampling process. The entire piston core was segmented at intervals of 2 cm to further analyze IRD and clay minerals.

Approximately 5 g of dried samples from core ANT34/A2-10 was accurately weighed and then separated by wet sieving (150 μm) after removal of carbonate and organic matter with 10% acetic acid and 3.5% hydrogen peroxide, respectively, to obtain the IRD component (Caniupán et al., 2011). The individual large particles were then removed from a few samples (mainly greater than 1 mm in our samples) to reduce the uncertainties caused by such large/massive particles in the counts and weight of the detrital particles. The number of particles (>150 μm) was counted under a binocular microscope (LEICA S8AP0), including the numbers of subangular to subrounded quartz, feldspar grains, and rock fragments, which could represent the IRD component (Teitler et al., 2010, Watkins et al., 1974, Starr et al., 2021). The weight percentage

(wt%) of the coarse fraction (>150 μm) to the weight of the dried bulk sample (Caniupán et al., 2011) was calculated as IRD wt%. Although radiolarian shells with sizes larger than 150 μm frequently appeared in the top layer (0-20 cm) of ANT34/A2-10, their weights were also much too low to contribute to the wt% of the >150 μm coarse-grained fraction record. Volcanic particles were not a significant component (rarely seen) in core ANT34/A2-10, most likely because ash plumes originated from the nearest volcanoes of the Peter I Island, which is located east of site ANT34/A2-10, and were typically transported and deposited eastward due to the prevailing strong Southern Westerly Winds (SWW) (Hillenbrand and Ehrmann, 2005).

Clay minerals from 227 samples were processed to obtain the <2 μm fraction, which was separated based on the conventional Stokes settling velocity principle after removing carbonate and organic matter by acetic acid and excess H_2O_2, respectively (Wan et al., 2010). X-ray diffraction (XRD) analysis of the sample was performed using oriented mounts with a D8 ADVANCE diffractometer manufactured by Brucker using CuKα radiation (40 kV, 40 mA) in the Key Laboratory of Marine Geology and Environment of the Institute of Oceanology, Chinese Academy of Sciences. The relative percentages of the leading clay mineral groups (smectite, kaolinite, illite, and chlorite) were estimated by weighting the integrated peak areas of the characteristic basal reflections in the glycolate state using Topas 2P software with the experimental factors published by (Biscaye, 1965). The relative proportions of kaolinite and chlorite were determined based on the ratio of the 3.58/3.54 Å peak areas in the glycolate state. The analytical precision (relative standard deviation) for the abundance of each clay mineral was estimated to be approximately ±5% (Wan et al., 2010). The illite chemical index was calculated from the ratio of the 5 Å and 10 Å illite peak areas in the glycolate state. Ratios higher than 0.4 represent Al-rich illite formed under strong hydrolysis, while ratios lower than 0.4 correspond to Fe-Mg illite, a product of the physical weathering of eroded rock (Ehrmann, 1998, Gingele et al., 2001).

The 6 bulk sediment samples (collect from IRD peak interval) were grounded under 200 mesh then transfer into the polytetrafluoroethylene (PTFE) solution flask after removing the carbonate and organic matter by 10 ml 0.25 mol/L HCl and excess H_2O_2, respectively. Then add 2 mL HF, 1.5 mL HNO_3 and 0.2 mL $HClO_4$ into the solution flask, tighten the cap, and heat it on an electric heating plate at 120°C for about a week until the sample in the bottle is completely dissolved. After the sample was dissolved completely, the lid was opened and steamed dry, and then the temperature was raised to 180 °C to remove the residual $HClO_4$. After evaporation, the sample was dissolved in 2.5 mol/L HCl and then transferred to a centrifuge tube. After centrifugation, we absorb the supernatant for further separation of Sr and Nd by using AG50W-X12 and P507 extraction resin ion-exchange columns, respectively. The Sr and Nd isotopes were tested and analyzed by a high-precision multi-reception plasma mass spectrometer (HRMC-ICP MS) produced by NU Company in the UK. And Sr and Nd isotopes were determined by NBS 981 ($^{87}Sr/^{86}Sr$=0.71033 ± 0.000008, 2σ) and NBS 987 ($^{87}Sr/^{86}Sr$=0.71031 ± 0.00003, 2σ), and Shin Etsu JNdi-1 ($^{143}Nd/^{144}Nd$=0.512115 ± 0.00005) standard sample to monitor the measurement quality (Tanaka et al., 2000, Steiger and Jäger, 1977). The analytical accuracy was within the range of ± 1%. The pretreatment and measurement were proceeding in the Key Laboratory of Marine Geology and Metallogeny, First Institute of Oceanography, Ministry of Natural and Resources.

Previous studies covering the late Quaternary in Antarctica have constrained ages by using correlations between surface water productivity proxies, such as biogenic opal/silica and Ti-normalized Ba concentration (measured directly or scanned by using XRF) and the LR04 $\delta^{18}O$ stack (Wu et al., 2017, Hillenbrand et al., 2009b, Ceccaroni et al., 1998, Tang et al., 2016, Presti et al., 2011). The age model of core ANT34/A2-10 has been established following this method through correlation of the XRF scanned Ba/Ti with the LR04 $\delta^{18}O$ stack, with two AMS ^{14}C age control points (fig. S1).

4 Results

4.1 Variations in IRD

Our IRD count result (grains per gram) largely parallels the weight result of >150 μm carbonate−free fraction (wt%) (fig. 2a). Most IRD consists of sand−sized quartz and feldspar grains with generally minor amounts of gravel in our sample. Both records show higher in interglacial and lower in glacial periods. To distinguish the peak of IRD, we first choose the IRD peak layer, which is characterized by the highest values of both the >150 μm wt% and the IRD grains per gram, and then use I1-I12 to represent the high IRD value periods in the interglacial time, which contains the IRD peak layer. These millennial−scale peaks reach values of counts up to ~640 grains per gram and ~3.6% (>150 μm wt%). The most pronounced peaks (the highest amplitude variation) occur at ~474-530 ka and 550-580 ka, represented by I7 and I8 in MIS 13 and 15, respectively (fig. 2a). Our IRD record shows millennial-scale variation patterns of IRD content over the last 773 ka in which nearly every IRD peak occurs in interglacial periods, while no IRD peaks occur in glacial periods.

4.2 Composition and parameters of clay minerals

For the last 773 ka, the clay-sized fraction of core ANT34/A2-10 consists mostly of smectite (30-59%) and illite (23-44%), while chlorite (5-22%) and kaolinite (1-16%) are present in lesser amounts. The variation patterns of kaolinite, illite, and chlorite are similar, showing higher values in the glacial periods (except for MIS 2) and lower values in the interglacial periods. However, kaolinite, illite, and chlorite show lower values during MIS 2 (figs. 2b-e). The opposite result occurs for smectite, which shows higher contents in the interglacial periods and lower contents in the glacial periods (smectite content is higher during MIS 2). Variations in chlorite and kaolinite contents are relatively small (~15%) but beyond the analytical limits (±5%) of the method used (Wan et al., 2017). Except for some high-frequency fluctuations after the MIS 6, the clay mineral parameters (smectite, kaolinite, illite, and chlorite content) display apparent glacial/interglacial oscillations; interglacial periods show higher values of smectite and lower values of kaolinite, illite, and chlorite, and glacial periods have lower values of smectite. Moreover, the higher values of

(smectite+kaolinite)/(illite+chlorite) ratios are consistent with the peaks in IRD during interglacial periods (fig. 2f). In contrast, the lower (smectite+kaolinite)/(illite+chlorite) ratios are common in glacial periods. All the samples display relatively narrow ranges of illite and smectite crystallinity values before MIS 6 while exhibiting relatively wide ranges of parameter values after MIS 6. The smectite and illite crystallinity range from 1-1.8 $\Delta 2\theta$ and 0.2-0.6 $\Delta 2\theta$, respectively, with fluctuations mainly around 1.3° $\Delta 2\theta$ and 0.3° $\Delta 2\theta$, respectively, indicating high to moderate crystallinity and very high to high crystallinity of smectite and illite, respectively (fig. 2g) (Ehrmann et al., 2005). The illite chemical index is less than 0.3, indicating strong physical weathering of the source area (fig. 2i) (Ehrmann, 1998, Wan et al., 2006, Gingele et al., 1998), and their lower values are common consistent with the IRD peak intervals. These results illustrate that our study area has a relatively stable detrital fraction source area, in which the source rocks are influenced by physical weathering. Meanwhile, this stepwise increasing and decreasing trend in all clay mineral parameters, consistent with IRD peak intervals, shows that they are systematically related and may suggest consistent changes in provenance variations during the G/IG cycles.

4.3 Strontium and neodymium isotopes

The Sr and Nd isotopic composition of the bulk sediment in the IRD peak interval is reported in table 1. The Sr isotope results (n=6, table 1) range from $^{87}Sr/^{86}Sr$=0.7106 to 0.7132 and $^{143}Nd/^{144}Nd$ (n=6, table 1) reveals values from 0.1524 to 0.1525. The significant shift of $^{87}Sr/^{86}Sr$ value appears in the IRD peak interval (I12) at about 760 ka.

5 Discussion

5.1 The iceberg flux variation related to the intensity of ocean-driven positive feedback

The widespread IRD deposited around the Southern Ocean and the southern subtropics could reflect Antarctica's long-term glacial evolution since the late Pliocene (Ehrmann et al., 1991). The contents of the IRD are usually considered to

reflect the iceberg flux from Antarctica (Kanfoush et al., 2000, Nielsen et al., 2007, Weber et al., 2014). Previous works suggest that increased iceberg survivability during periods of widespread sea ice and increased iceberg flux from Antarctica determined the transport of IRD within the Southern Ocean (Nielsen and Hodell, 2007), and the IRD deposition close to Antarctica is generally highest during interglacial periods and periods of ice-sheet retreat (Weber et al., 2014). In contrast, IRD maxima typically occur during glacial periods at Subantarctic Zone (Starr et al., 2021). Site ANT34/A2-10 is located near the modern SACCF and is strongly influenced by the relatively warmer ACC; the current passes through the Drake Passage and then steers icebergs toward the east and causes the water at site ANT34/A2-10 to be generally warmer than the Southern Ocean, melting local icebergs (Orsi et al., 1995). This contrast generally leads to low survivability for icebergs under the present warm period at site ANT34/A2-10 (Weber et al., 2014). However, the unstable and disintegrated WAIS could generate sufficient iceberg flux to reach this distal site ANT34/A2-10 in warm periods, leading to higher iceberg survival and contributing to the IRD peak intervals in interglacial periods. This vulnerability of WAIS may be caused by increasing ocean-driven positive feedback processes, which involve the upwelling of warm, well-ventilated CDW and the intense ice mass loss process with the WAIS instability. In contrast, high survivability for icebergs may prevail during glacial periods, in which the tropicward shift of the SWW drives the SACCF to the north, and the water at site ANT34/A2-10 is generally as cold as the coastal Southern Ocean (Hillenbrand et al., 2009b). This condition may contribute to the survival of past glacial sediment-laden iceberg in the Amundsen Sea, thus release less IRD in the study region than in the warm period.

The intense glacial deep water stratification could increase regenerated nutrients in the deep and reduce preformed nutrients in intermediate water masses (Toggweiler et al., 2006), and produces a stronger chemical stratification between southern sourced deep and intermediate waters (Ziegler et al., 2013). This mechanism lets the benthic foraminiferal calcite $\delta^{13}C$ gradients reconstruct the chemical stratification/deep water

ventilation between the deep and intermediate ocean (Charles et al., 2010, Ullermann et al., 2016, Hall et al., 2001). Our results show that the peaks of iceberg flux in core ANT34/A2-10 are well correlated with the minimum benthic $\delta^{13}C$ gradient ($\Delta\delta^{13}C_{(1088-849)}$) and the peaks of accumulation rate in EDC ice core, which may relate to the intense ventilation of warm CDW (Hodell et al., 2003, Ullermann et al., 2016) and the intense westerly wind-driven upwelling of warm CDW (Members, 2013), respectively, since 773 ka (figs. 3a-c). We suggest that this correlation could be explained by positive feedback processes as follow. The well-ventilated warm CDW could upwelling and intrude into the Antarctic shelf region in the South Pacific Southern Ocean (Jacobs et al., 1996, Thoma et al., 2008, Dinniman et al., 2012, Schmidtko et al., 2014), resulting in enhanced iceberg calving and exacerbating the basal melting process by warming the subsurface ocean adjacent to the SPS of WAIS, increasing the instability of WAIS (Adusumilli et al., 2020, Davis et al., 2018, Hansen et al., 2016, Liu et al., 2015). Meanwhile, the intense ice mass loss in SPS of WAIS could supply vast amounts of meltwater to the surface layer of the Southern Ocean, contributing to the upper ocean stratification and maintaining the heat in the subsurface ocean, then warming the vulnerable WAIS continuously and causing its further disintegration (Davis et al., 2018, Jacobs et al., 2011, Walker et al., 2007, Fogwill et al., 2015). Moreover, this process might have cooled the surface waters near the Antarctic continent by isolating the surface and warm subsurface ocean (Bronselaer et al., 2018), which may allow the icebergs to transport equatorward without significant melting until they reached the south boundary of warmer ACC (Hillenbrand et al., 2009b). Our core site ANT34/A2-10 may locate at the north of SACCF during these periods. The variations in increasing upwelling of well-ventilated CDW are consistent with the higher frequency and significance of the IRD content variations in our core affirmed the vigorous intensity of ocean-driven positive feedback related to the vulnerability of the WAIS. In contrast, the absence of IRD peaks in glacial periods at site ANT34/A2-10 may indicate the weak intensity of ocean-driven positive feedback in the South Pacific Ocean. Furthermore, the dense

water generated in the Ross Sea shelf region may have suppressed the intrusion of MCDW into the base of the Ross Ice Shelf (Schmidtko et al., 2014), also weakening the intensity of ocean-driven positive feedback during glacial periods.

We also notice that the extreme high IRD peak, representing high iceberg flux, occurs from MIS 13 and 15 before the Mid-Brunhes Event, which represents a vital climate transition occurring at approximately 430 ka. Furthermore, this specific pattern of changes in IRD has also been found elsewhere around Antarctica (Hillenbrand et al., 2009b, Caburlotto et al., 2009), which may be associated with cooler interglacials, including MIS 13 and 15, than the more recent interglacials, with the unusual warmth of the glacial MIS 14 as recorded by the EDC ice core (fig. 3c) (Jouzel et al., 2007). We suggest that the cooler condition of the surface cryosphere in MIS 13 and 15 may be suitable for the survival of the Antarctic-origin iceberg, while the warmer condition in MIS 14 may contribute to the extra ice mass loss process (including iceberg calving and basal melting) without the ocean-driven forcing. Moreover, these processes may contribute to the refreshing event of the surface water in the south Pacific and south Atlantic Southern Ocean during MIS 13-15, which was documented by the relatively low planktonic $\delta^{18}O$ ratios observed in both the Amundsen and the Weddell Sea during MIS 14 (Hillenbrand et al., 2009b). In addition, the terrestrial margins of the Antarctic Ice Sheet are sensitive to local summer insolation (Pollard and DeConto, 2009, Patterson et al., 2014), and MIS 13 had been subjected to strong isolation forcing, which may drive additional ice mass loss and enhance the Antarctic interglacial periods (Tigchelaar et al., 2018, Wu et al., 2021) (further discussion in section 5.3). Therefore, we suggest that the large iceberg flux in site ANT34/A2-10 at MIS 13 and 15 may be caused by 1) increasing ocean-driven ice mass loss; 2) the high iceberg survivability caused by the lower amplitude of the Antarctic temperature anomaly (fig. 3c); 3) local summer insolation maximum, which may drive additional ice mass loss of the ice sheet and generate more icebergs in MIS 13 and 15 (figs. 3a and f).

5.2 Iceberg provenance variation during G/IG cycles

Site ANT34/A2-10 is far from the Amundsen Sea hinterland, which means that the clay minerals cannot be supplied by the glaciers adjacent to the ASE, and little dust/current is imported from the same source areas in the western Antarctic (Petschick et al., 1996, Hillenbrand et al., 2003). Therefore, drifting sediment-laden icebergs may be the primary carriers of clay-sized fractions in the Amundsen Sea (Hillenbrand et al., 2003). Since the mineralogical trends and the relative compositional differences in clay-sized mineral assemblages can constrain the provenances of sediment, we can diagnose the source of specific sediment-laden icebergs in the Southern Ocean (Hillenbrand et al., 2009a, Krylov et al., 2008).

A primary assumption is that the sources of clay minerals in the Amundsen Sea may not have changed significantly during the study time, which is reasonable because there has been no notable tectonic activity around the SPS of West Antarctica at least since the early Pleistocene (Hillenbrand and Ehrmann, 2005, Perez et al., 2021). Thus, the provenance of drifting sediment-laden icebergs may also not have changed significantly since this time. However, during Quaternary G/IG cycles, there have been periods of extensive land ice across the sub-Antarctic both on islands scattered north of the SACCF and near Patagonia, providing alternative sources for debris-carrying icebergs in the South Pacific Southern Ocean (Bigg, 2020). Our interpretation could be supported by the smectite crystallinity (1-1.8° $\Delta 2\theta$), illite crystallinity (0.2-0.6° $\Delta 2\theta$), and illite 5/10 Å (0.1-0.3) in core ANT34/A2-10, which are comparable to the average smectite and illite crystallinity, and illite 5/10 Å ranges from 1-1.6° $\Delta 2\theta$, while the illite crystallinity ranges from 0.2-0.7° $\Delta 2\theta$ of clay minerals from the Transantarctic Mountains (Ehrmann et al., 2005). In addition, studies show that the clay-sized fraction deposited in the Amundsen Sea includes multi-sourced particles that originated from different regions, including Marie Byrd Land, Ellsworth Land, and the Antarctic Peninsula (Hillenbrand et al., 2003, Ehrmann et al., 2005, Ehrmann et al., 2011). Therefore, we need to find a useful diagnostic clay mineral-related proxy for better discrimination of the potential endmembers to identify the different sources of iceberg mixtures in the study area.

We note that core ANT34/A2-10 is characterized by a relatively high kaolinite content (fig. 2b). However, current climatic conditions, which dominated Antarctica since the establishment of the Cenozoic cryosphere in the early Oligocene with intense physical weathering, do not provide pedogenic kaolinite (Ehrmann et al., 1992). Therefore, the relatively high kaolinite concentrations in core ANT34/A2-10 may suggest pre-Oligocene sedimentary rocks or paleosols in the source area, and the kaolinite has not been destroyed by metamorphism or deep burial processes (Hillenbrand et al., 2003). Previous studies have indicated that relatively higher kaolinite and smectite contents in the ASE are potential indicators of contributions from Marie Byrd Land and Peter I Island, respectively (Ehrmann et al., 2011, Hillenbrand et al., 2003). In contrast, the contributions of clay minerals from north Victoria Land and the RSE appear to contain relatively low to no kaolinite but abundant smectite (Pant et al., 2013, Setti et al., 2004, Graly et al., 2020), and all of these regions have relatively high illite and chlorite contents. Meanwhile, north Victoria Land and the RSE typically have higher kaolinite+smectite (mainly because of the high values of smectite in Transantarctic Mountains detritus) and lower illite+chlorite values than the ASE. Moreover, kaolinite is absent in the RSE (Ehrmann et al., 2005), and the kaolinite+smectite and illite+chlorite contents are profoundly different between these embayments. Therefore, we suggest that clay mineral endmembers of kaolinite+smectite, illite, chlorite, and the (kaolinite+smectite)/(illite+chlorite) ratio may be useful diagnostic proxies to identify the mixture of icebergs from the RSE and the ASE in the study area. Based on this interpretation, we draw ternary diagrams of smectite-kaolinite-illite+chlorite (fig. 4a) and determine that the provenances of sediment-laden icebergs at site ANT34/A2-10 involved both the ASE and RSE (fig. 1b). Clay minerals assembled in core ANT34/A2-10 are very similar to the sample site in ASE and RSE sediments; this result can be interpreted as a mixture of multiple sediment-laden icebergs with sources from the ASE and RSE in site ANT34/A2-10. However, the icebergs at site ANT34/A2-10 have quite different provenances from those of the ASE and RSE and/or north Victoria Land (fig. 4a) between IRD peak intervals and low

IRD content intervals.

The ternary diagram shows that clay mineral assemblages in the IRD peak intervals at site ANT34/A2-10 during the interglacial periods were mixed with clay minerals from the ASE and RSE; however, the ASE was the main source of clay minerals during the low IRD content interval in glacial periods (fig. 4a). Our interpretation also supports by the Sr-Nd isotopic composition in bulk sediment of ANT34/A2-10 at IRD peak interval, which has a similar Sr-Nd isotopic composition with the glacial drift (include dolerite, sandstone, and granite) in the hills and valleys in the north and/or south Victoria Land, respectively (fig 4b). These results indicate that site ANT34/A2-10 could receive sediment-laden icebergs both from the ASE and the RSE in IRD peak intervals during interglacial periods since 773 ka. However, site ANT34/A2-10 may receive fewer icebergs from ASE during glacial times. Alternatively, the ASE originate sediment-laden icebergs may survive at site ANT34/A2-10 and led to less IRD input during glacial periods. Moreover, the clay mineral assemblage indicates a mixture of icebergs from the ASE and north Victoria Land, East Antarctica, around the end of the MIS 18 (fig. 4a). Our result shows that these variations in clay mineral assemblages may be controlled by different transport patterns for iceberg trajectories, which is also well reflected by the variations in (kaolinite+smectite)/(illite+chlorite) (figs. 3a and d). The high values of (kaolinite+smectite)/(illite+chlorite) accompanying the IRD peaks (I1-9) indicate the mixture of clay minerals from RSE and ASE and imply a mixture of icebergs from the ASE and the RSE at the IRD peak intervals during interglacial periods. Furthermore, the high values of this ratio accompanying the IRD peaks (I10-12) imply the mixture of icebergs from the north Victoria Land, RSE, and ASE around MIS 18 (figs. 4a and b). We suggest that these variations in iceberg provenance may be explained by abrupt shifts in the Amundsen Sea low-pressure system (ASL). As a highly dynamic and mobile climatological low-pressure system located in the South Pacific Southern Ocean, the ASL is a crucial driver of West Antarctic climate variability that may accelerate glacial ice (Hosking et al., 2016). Additionally, the longitudinal shift in the ASL could strongly influence the

surface climate by controlling the meridional winds directed toward West Antarctica (Phillips et al., 2013, Wang et al., 2020, Turner et al., 2013). Thus, the shift in ASL can influence the local atmospheric circulation and then the iceberg trajectory in South Pacific Southern Ocean.

In the interglacial period scenario, the southwestward shift of the ASL would lead to a poleward shift in the SWW, which could have caused the poleward movement of the SACCF compared to its modern position (Turner et al., 2013, Hosking et al., 2016, McCulloch et al., 2020). In this case, site ANT34/A2-10 could strongly be influenced by the ACC. Moreover, those icebergs calved from the Ross Ice Shelf front may be transported by a clockwise coastal AASW to the north and then pushed by the SWW toward the east to pass site ANT34/A2-10 (figs. 5a) (Baines and Fraedrich, 1988). The close correlation between IRD peaks well evidences this interpretation in core ANT34/A2-10 and high ice accumulation rates in EDC, which indicates the poleward shift of SWW (figs. 3a and e) (Members, 2013). In the glacial period scenario, the northeast shift in the ASL could lead to a tropicward shift of the easterlies accompanying the tropicward movement of the SWW and SACCF (Hosking et al., 2016, McCulloch et al., 2020). In this case, site ANT34/A2-10 may not be influenced by the ACC and suitable for icebergs survival. Furthermore, weak ocean-driven positive feedback may lead fewer icebergs to calve from the front of the glacier, and the ice shelf adjacent to the ASE, then these icebergs carried by a clockwise coastal current near the ASE hinterland and transported to the north, and finally passing over site ANT34/A2-10 (fig. 5b). This interpretation is supported by the correlation between the low IRD content linked with low values of (kaolinite+smectite)/(illite+chlorite) (less than 0.9) and low accumulation rates in the glacial periods (figs. 3a, c, and d). However, all the IRD peaks (I10-12) in the interglacial or glacial periods (around MIS 18) coincide with higher values of (kaolinite+smectite)/(illite+chlorite) and increasing trends in the accumulation rate. These results may be related to the abrupt southwestward shift in the ASL during this period (Konfirst et al., 2012). This shift in the ASL is responsible for an abrupt

poleward shift in the easterlies and westerlies, which may allow icebergs to travel from the north Victoria Land to site ANT34/A2-10 with the prevailing SWW and westerly flow (Baines and Fraedrich, 1988) (fig. 5a).

5.3 Vulnerability of WAIS in SPS

Today, the vulnerability of WAIS is mainly caused by warm CDW and/or MCDW intrusion into the shelf region adjacent to the SPS of the WAIS (Jacobs et al., 1996, Lowe and Anderson, 2002, Dinniman et al., 2012, Das et al., 2020, Adusumilli et al., 2020, Nakayama et al., 2018), which is tightly related to the enhanced iceberg melting in this sector (Bronselaer et al., 2018). Our results show a clear correlation between $\Delta\delta^{13}C_{(1088\text{-}849)}$ and IRD peaks in core ANT34/A2-10 (figs. 3a and b). These results indicate that an increasing iceberg flux (intensified ice loss) was caused by strengthening upwelling of warm, well-ventilated CDW since 773 ka BP. The relatively good correlations between IRD content, (kaolinite+smectite)/(illite+chlorite), $\Delta\delta^{13}C_{(1088\text{-}849)}$, and EDC accumulation rate (fig. 3) support an assumption that the poleward shift in the intense SWW accompanied by the deepening of ASL may have triggered the increased upwelling of well-ventilated relatively warm CDW, warming the subsurface ocean then causing the calving of icebergs from the front of the GIS and TG, with Ross Ice Shelf in the ASE and RSE, respectively (Hillenbrand et al., 2009b, Turner et al., 2013, Menviel et al., 2010, Members, 2013). Moreover, in the interglacial period scenario, this poleward shift of intense SWW accompanying the deepening of ASL may relate to the positive Southern Annular Mode (Turner et al., 2013), which could lead to the cooling of the sea surface in the south of SACCF and substantially alter the Southern Ocean circulation patterns, diminishing the absorption of CO_2 (Lovenduski, 2005, Sen Gupta and McNeil, 2012). It may contribute to iceberg survival during their transportation before they reach the ACC. Furthermore, the increased upwelling of well-ventilated relatively warm CDW, led to the retreat of the grounding line and the influx of meltwater delivered into the South Pacific Southern Ocean (through the basal melting, iceberg calving and breakup process) with the loss ice volume (England et al., 2020).

522 This process could have stabilized the upper water column by shoaling the halocline
523 and/or thermocline in the South Pacific Southern Ocean, maintaining the heat budget
524 in the subsurface ocean that could cause the warming of the subsurface ocean and
525 finally destabilize the WAIS (fig. 6a) (Richardson, 2005, Schmidtko et al., 2014,
526 Menviel et al., 2010). These systematic processes are also supported by the previous
527 record in 'Iceberg Alley' and are consistent with the climate model simulations of the
528 period since the recent G/IG cycle (Weber et al., 2014) and consist with the
529 documented fresh meltwater input event in the study region during MIS 13-15
530 (Hillenbrand et al., 2009b). In contrast, in the glacial period scenario, a northeastward
531 shift in the ASL was accompanied by a tropicward shift in easterlies and SWW, which
532 led to the reduced wind-driven warm deep water intrusion to the Amundsen shelf
533 region, thereby deepening the halocline and/or thermocline in South Pacific Southern
534 Ocean. These systematic processes may contribute to the stability of WAIS (fig. 6b).
535 Our spectrum and wavelet analysis of IRD records (count number) show significantly
536 high power during the period of 41 ka (higher power before around 400 ka BP than
537 after 400 ka BP on 41 ka band) and 100 ka (see supplementary material figs. S3a, b).
538 Moreover, we use the 'Cross wavelet and wavelet coherence toolbox' for MATLAB
539 (Grinsted et al., 2004) to perform the cross-wavelet coherency (XWT) analysis
540 between IRD record with obliquity and eccentricity (Laskar et al., 2004). The result
541 shows an in-phase relationship between IRD record and eccentricity (see
542 supplementary material figs. S3c), with a different leading relationship between IRD
543 record and obliquity before and after 400 ka BP. Additionally, the IRD peaks and its
544 eccentricity bandpass filter result show a good correlation with the eccentricity
545 maximum (figs. 3a and g). These results may implicate that the Antarctic Ice sheet
546 variation was mostly driven by CO_2 and sea level forcing with a period of 100 ka
547 cycle (Tigchelaar et al., 2018, Huybrechts, 2002) and may relate to the obliquity
548 pacing onset of the glacial termination during the late Pleistocene (see supplementary
549 material fig S3d and e) (Huybers and Wunsch, 2005, Huybers, 2007). Also, the
550 obvious pacing of IRD peaks by obliquity after around 400 ka BP was documented in

the south Atlantic ocean (Starr et al., 2021), which consists with our result (figs. S3 d and e).

However, the variation in eccentricity/obliquity does not explain the causes of extremely high IRD peaks of I7-9 in MIS 13 and 15, which represent the periods of greatest WAIS instability because the repeated eccentricity maximum after 400 ka does not accompany the same extreme high IRD peaks such like in MIS 13 and 15. We suggest that, this phenomenon may be due to 1) the more extended interglacial periods before the Mid-Brunhes Event (MIS 13, 15, and 17), which was characterized by larger ice sheets, lower sea level, and cooler temperatures in Antarctica than the more recent interglacial periods (MIS 5, 7, 9, and 11) (Oliveira et al., 2020), and 2) intense local summer insolation, which may drive additional ice mass loss over the Antarctic ice shelves (Tigchelaar et al., 2018, Wu et al., 2021). Based on the XWT and WTC analysis between the IRD count number and 75°S summer insolation, we found that nearly every IRD period shows a significant correlation with 75°S summer insolation (figs. 3h and i). However, only the IRD peak intervals I7-9 in MIS 13 and 15 show both the significant correlation and coherence with the phase relationship with 75°S summer insolation. These results could support the conclusion intense local summer insolation combines with the lower amplitude of the Antarctic temperature anomaly in MBE (MIS 13 and 15) may drive additional ice mass loss processes and cause the further destabilization of WAIS.

6 Conclusion

This study provides the first long-term sedimentological evidence of ocean-driven positive feedback in the South Pacific Southern Ocean and its relationship with the low-pressure system in the high-latitude cryosphere. Based on multiple proxies, our results show that an increase in IRD always accompanies the enhanced upwelling of well-ventilated deep water in the Southern Ocean at site ANT34/A2-10. The changes in relatively warm CDW and/or MCDW upwelling on the millennial scale are closely related to iceberg calving variations, basal melting, and meltwater input, significantly affecting WAIS stability variations. The ASL has a strong influence on meridional

580 atmospheric circulation in the Southern Ocean and thus could exert a strong influence
581 on the trajectories of icebergs. The clay mineral and Sr-Nd isotopic compositions in
582 IRD peak intervals show that its provenance significantly switches abruptly due to the
583 variability of the ASL position during G/IG cycles. When ASL shifts to the northeast
584 accompany with the SWW, and prevailing easterlies move tropicward during glacial
585 periods, fewer icebergs are transported to supply site ANT34/A2-10 through the
586 clockwise AASW along the shore. In this case, site ANT34/A2-10 (near the modern
587 SACCF) may not be influenced by the SWW and ACC and only receive the iceberg
588 from ASE. However, during interglacial periods, ASL shifts to the southwest
589 accompany with the SWW and prevailing easterlies move poleward. In this case, the
590 icebergs generated by the Ross Ice Shelf and the nearby glaciers on the north and
591 south Victoria Land are transported eastward and mix with the icebergs that are calved
592 from the ice sheet adjacent to the ASE. The WAIS evolution is closely related to
593 obliquity and eccentricity. However, the increasing 75°S summer insolation and weak
594 Antarctic temperature variability accompany the increasing ocean-driven process,
595 leading to the additional iceberg flux, resulting in the high-frequency variation and the
596 highest IRD peak intervals in MIS 13 and 15.

597 **Table 1. Sr and Nd isotopic compositions bulk sediment samples from core**
598 **ANT34/A2-10.**

Depth (cm)	IRD peak interval	Age (ka BP)	$^{143}Nd/^{144}Nd$	SE	$^{87}Sr/^{86}Sr$	SE
After the end of the Middle Pleistocene climatic transition (around 700 ka)						
34-36	I2	47.8	0.512508	0.000004	0.710617	0.000004
54-56	I3	83.7	0.512506	0.000006	0.710498	0.000004
60-62	I3	101.4	0.512466	0.000003	0.710463	0.000005
268-270	I7	507.6	0.512446	0.000003	0.710390	0.000005
310-312	I9	572.8	0.512459	0.000004	0.710612	0.000007
Before the end of the Middle Pleistocene climatic transition (around 700 ka)						
420-422	I12	759.3	0.512422	0.000004	0.713249	0.000007

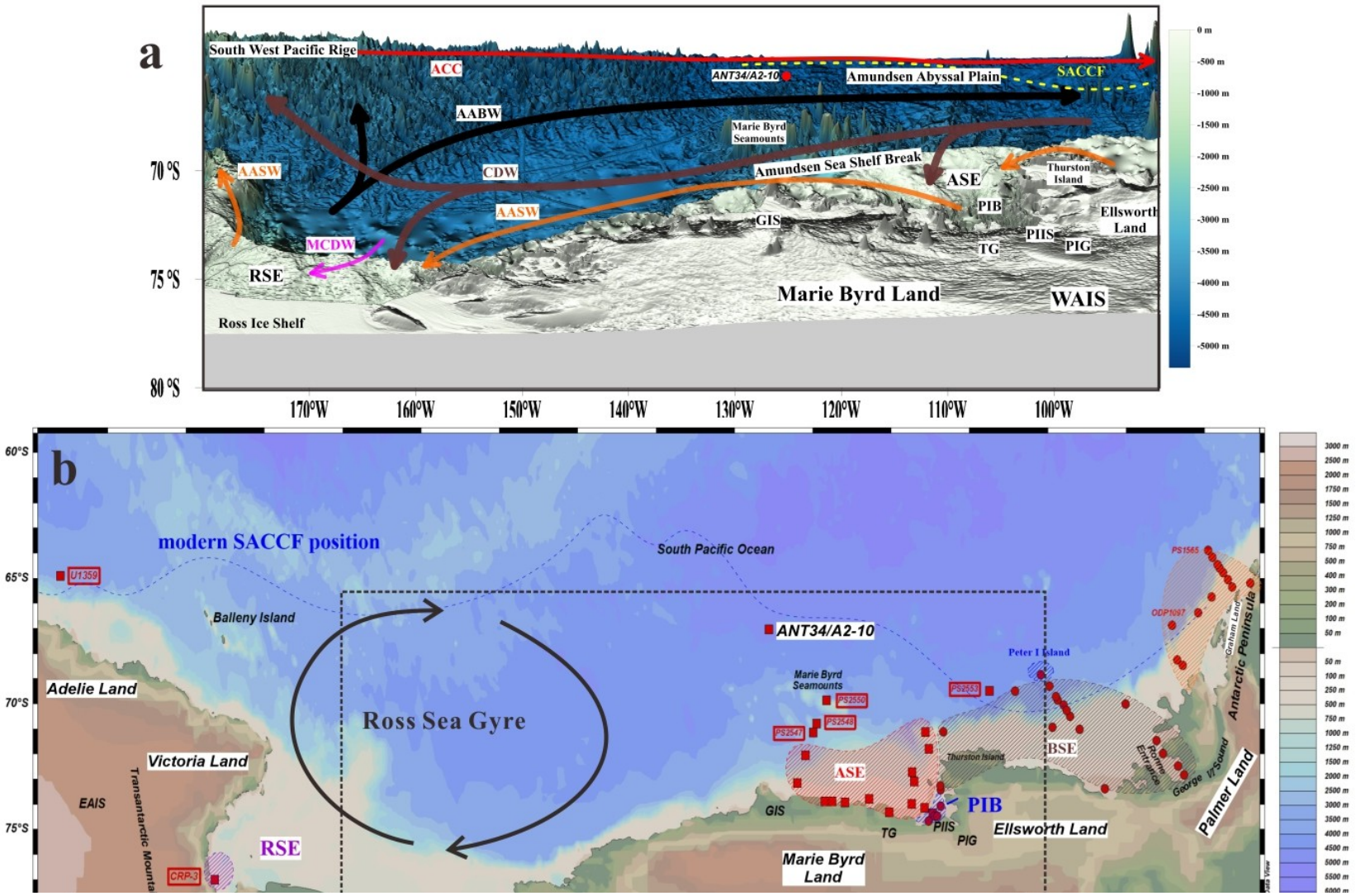
a
South West Pacific Rige
ACC
ANT34/A2-10
Amundsen Abyssal Plain
SACCF
AABW
Marie Byrd Seamounts
AASW
CDW
Amundsen Sea Shelf Break
ASE
Thurston Island
PIB
Ellsworth Land
GIS
PIIS
PIG
TG
MCDW
RSE
Marie Byrd Land
WAIS
Ross Ice Shelf
70 °S
75 °S
80 °S
170°W
160°W
150°W
140°W
130°W
120°W
110°W
100°W
0 m
-500 m
-1000 m
-1500 m
-2000 m
-2500 m
-3000 m
-3500 m
-4000 m
-4500 m
-5000 m
b
modern SACCF position
South Pacific Ocean
U1359
Balleny Island
ANT34/A2-10
Peter I Island
PS1565
ODP1097
Graham Land
Antarctic Peninsula
Adelie Land
Marie Byrd Seamounts
PS2550
PS2551
PS2547
PS2548
Ross Sea Gyre
Thurston Island
BSE
Victoria Land
ASE
Bellingshausen Sea
George VI Sound
Palmer Land
EAIS
Transantarctic Mountains
GIS
PIB
TG
PIIS
PIG
Ellsworth Land
RSE
CRP-3
Marie Byrd Land
60°S
65°S
70°S
75°S
3000 m
2500 m
2000 m
1750 m
1500 m
1250 m
1000 m
750 m
500 m
400 m
300 m
200 m
100 m
50 m
50 m
100 m
250 m
500 m
750 m
1000 m
1250 m
1500 m
2000 m
2500 m
3000 m
3500 m
4000 m
4500 m
5000 m
5500 m
6000 m

Figure 1. Location map. a, geographic and oceanographic information of the study area; b, the location of the sites with the clay mineral and Sr-Nd endmember data from references.

WAIS: West Antarctic Ice Shelf, EAIS: East Antarctic Ice Sheet, ASE: Amundsen Sea embayment, RSE: Ross Sea embayment, BSE: Bellingshausen Sea embayment, GIS: Getz Ice Shelf, TG: Thwaites Glacier, PIB: Pine Island Bay, PIG: Pine Island Glacier, PIIS: Pine Island Ice Shelf, ACC: Antarctic Circumpolar Current, AABW: Antarctic Bottom Water, CDW: Circumpolar Deep Water, MCDW: Modified Circumpolar Deep Water, AASW: Antarctic Surface Water, SACCF: South Antarctic Circumpolar Current Front. The position of the SACCF is modified from (Benz et al., 2016). Dash line indicate the study area.

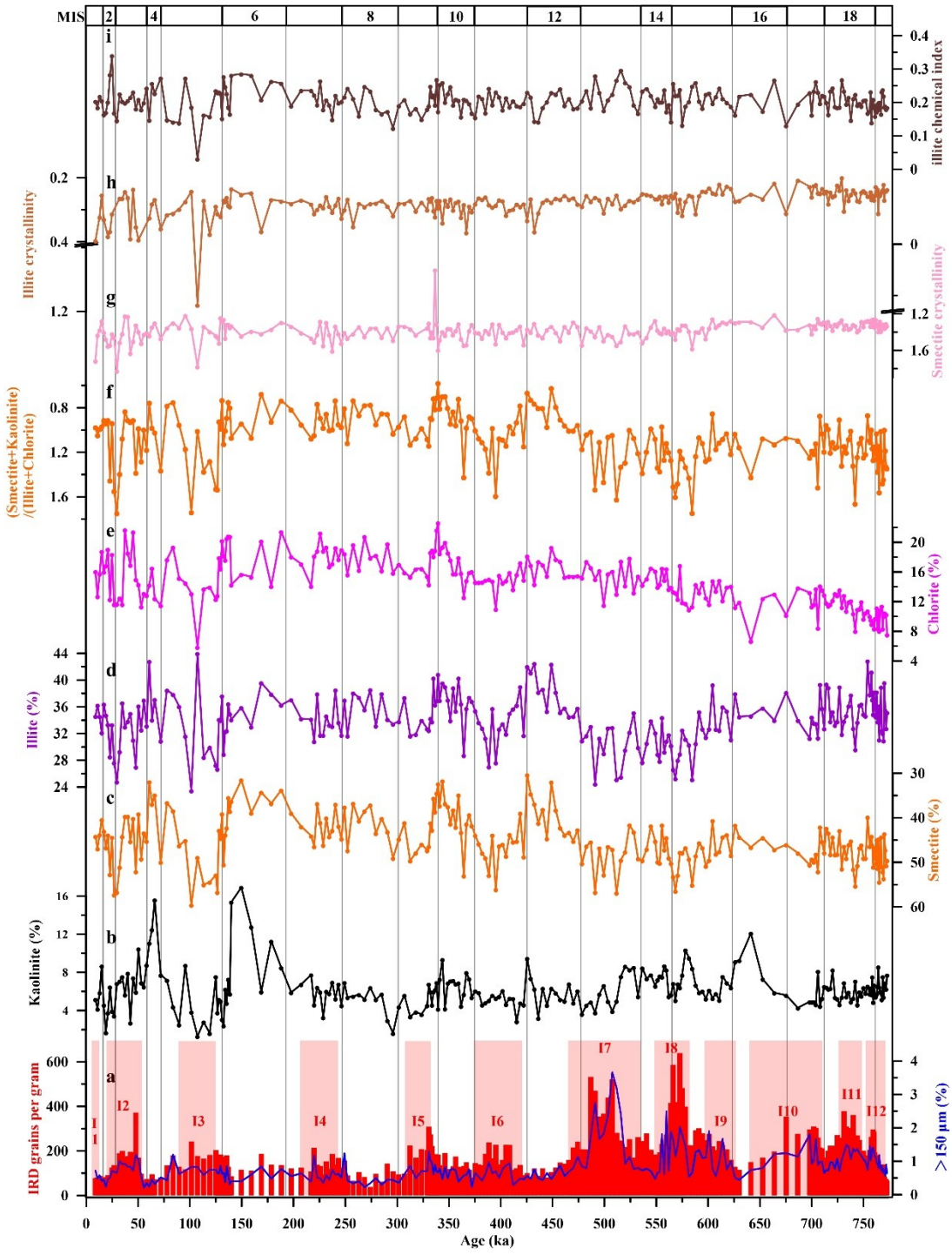

Figure 2. Down core variation patterns of IRD content and clay mineral parameters.

The numbered series of IRD peaks are I1-12, where the letter I means interglacial periods. The gray lines indicate the boundaries of the G/IG cycles.

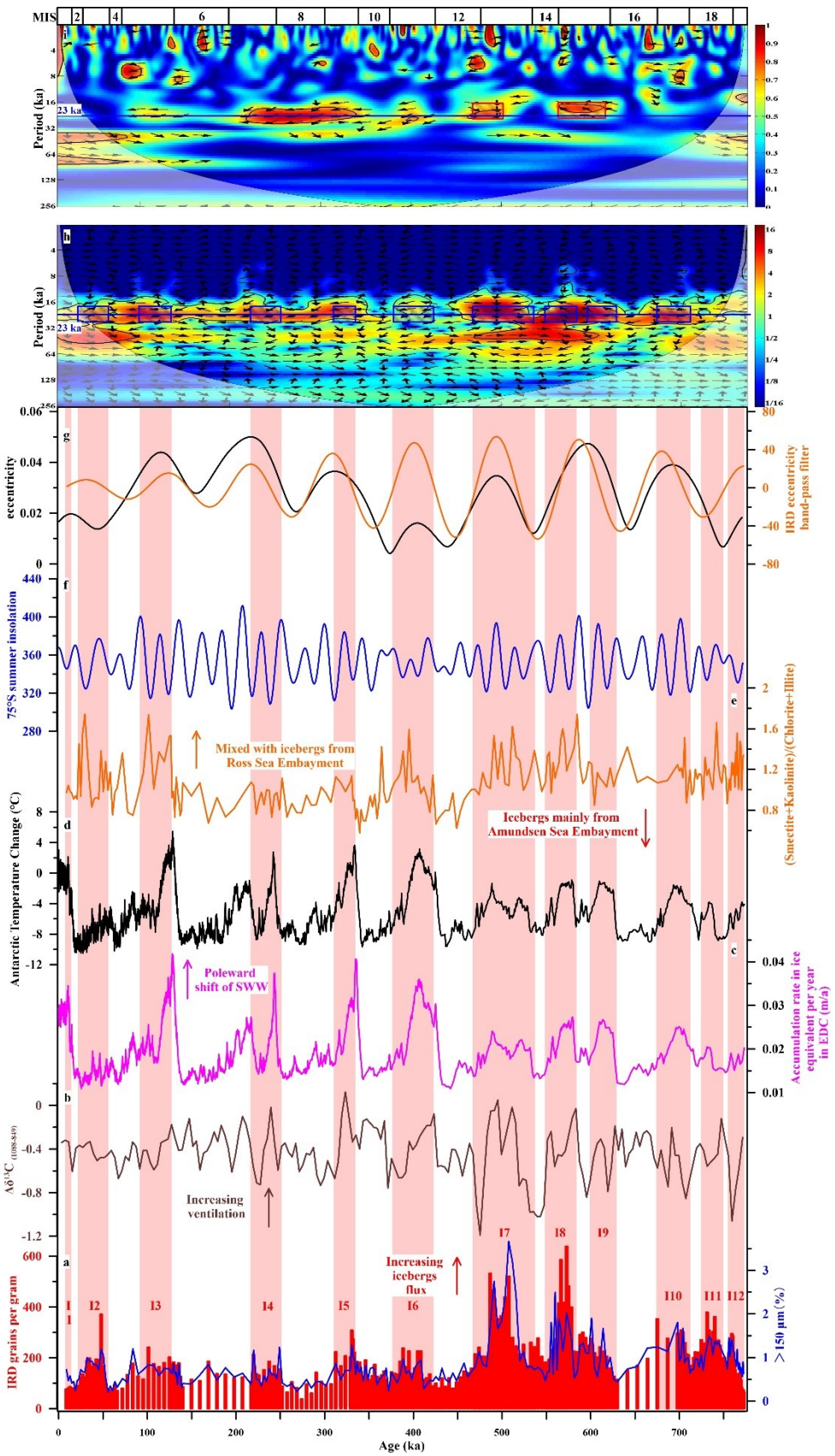
MIS
Period (ka)
23 ka
eccentricity
IRD eccentricity band-pass filter
75°S summer insolation
(Smectite+Kaolinite)/(Chlorite+Illite)
Mixed with icebergs from Ross Sea Embayment
Icebergs mainly from Amundsen Sea Embayment
Antarctic Temperature Change (°C)
Poleward shift of SWW
Accumulation rate in ice equivalent per year in EDC (m/a)
Increasing ventilation
Increasing icebergs flux
IRD grains per gram
>150 μm (%)
I1
I2
I3
I4
I5
I6
I7
I8
I9
I10
I11
I12
Age (ka)

612

Figure 3. Proxies in our study of core ANT34/A2-10 with the cross-wavelet coherency (XWT) and wavelet coherence (WTC) analysis between IRD and summer insolation since 773 ka BP.

From bottom: a, IRD proxies in core ANT34/A2-10; b, benthic $\delta^{13}C$ gradient of the south Atlantic-east equatorial Pacific ($\Delta\delta^{13}C_{(1088\text{-}849)}$), data from (Mix et al., 1995, Hodell et al., 2003); c, EDC temperature anomaly (Jouzel et al., 2007); d, clay mineral ratio of (kaolinite+smectite)/(illite+chlorite) in ANT34/A2-10; e, accumulation rate in ice equivalent per year in the EDC (Wolff et al., 2010); f, 75°S summer insolation; g, the result of IRD eccentricity bandpass filter calculates by software 'Acycle' (Li et al., 2019) (orange line) and orbital eccentricity (black line); h, i, XWT and WTC analysis between the result of IRD count number and 75°S summer insolation, respectively. The orbital parameters are from (Laskar et al., 2004). Red shading represents interglacial periods with IRD peaks. The blue line in h and i represents the 23 ka orbital bands, and the relative phase relationship is shown as black arrows. The thin contour in (h and i) indicates the false-alarm level 95% against red noise, and the cone of influence where edge effects might distort the picture are shown in a lighter shade. The original data of ODP 1088 and the original time series of ODP 849 were both resampled in 4 ka spacing with a linear interpolation method between data points before calculation their difference value. The program Past V3.5 (Hammer and Harper, 2008) use for resampling these data.

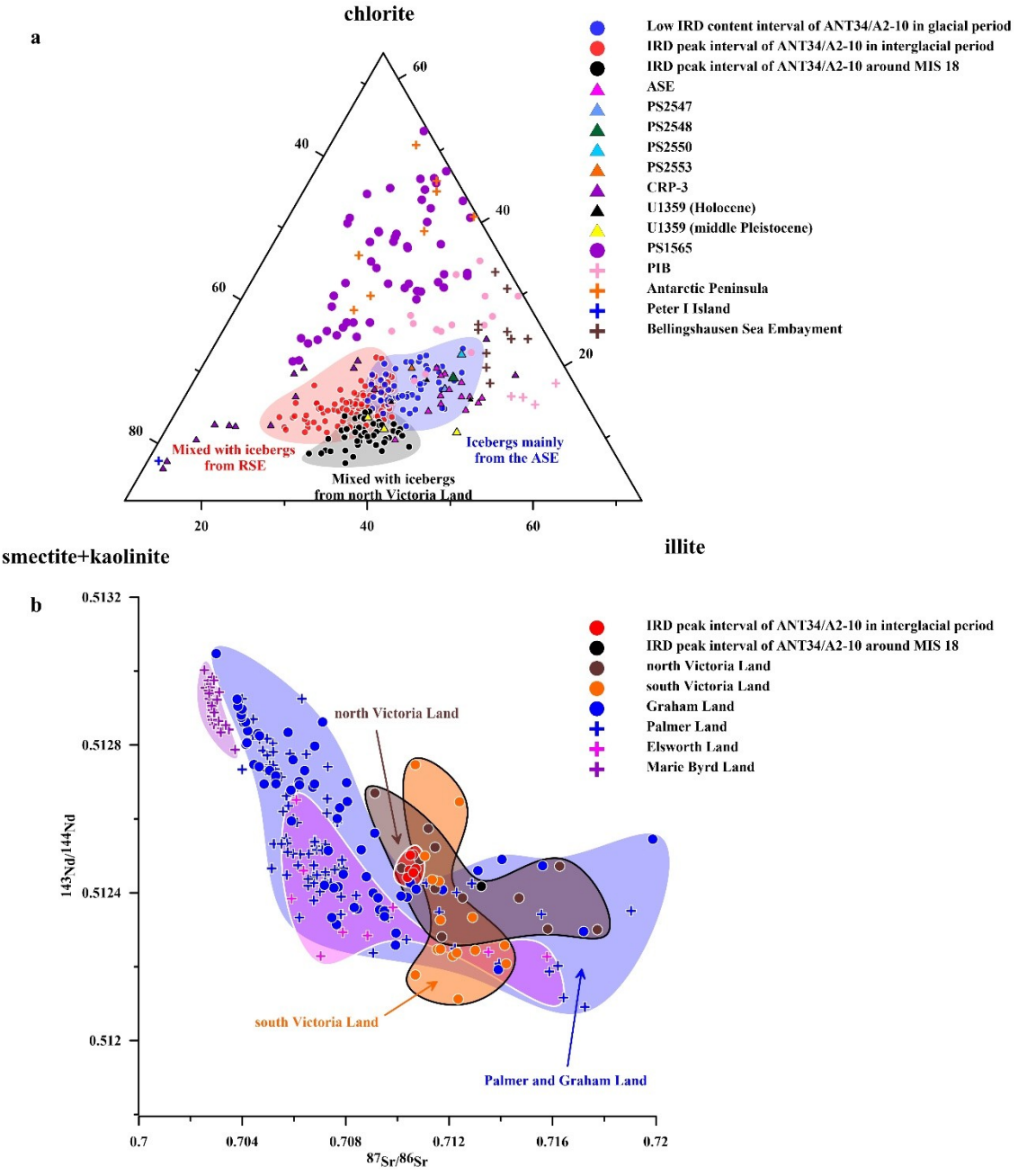
a
chlorite
smectite+kaolinite
illite
Low IRD content interval of ANT34/A2-10 in glacial period
IRD peak interval of ANT34/A2-10 in interglacial period
IRD peak interval of ANT34/A2-10 around MIS 18
ASE
PS2547
PS2548
PS2550
PS2553
CRP-3
U1359 (Holocene)
U1359 (middle Pleistocene)
PS1565
PIB
Antarctic Peninsula
Peter I Island
Bellingshausen Sea Embayment
Mixed with icebergs from RSE
Icebergs mainly from the ASE
Mixed with icebergs from north Victoria Land
b
IRD peak interval of ANT34/A2-10 in interglacial period
IRD peak interval of ANT34/A2-10 around MIS 18
north Victoria Land
south Victoria Land
Graham Land
Palmer Land
Elsworth Land
Marie Byrd Land
north Victoria Land
south Victoria Land
Palmer and Graham Land
143Nd/144Nd
87Sr/86Sr

633

Figure 4. Endmember analysis of clay mineral and Sr-Nd isotopes in core ANT34/A2-10.

a, ternary diagram of smectite+kaolinite-illite-chlorite shows variations in clay mineral compositions during low IRD content interval in glacial and IRD peak interval in interglacial periods and the period around the MIS 18. b, Sr-Nd isotopic compositions of core ANT34/A2-10 during IRD peak interval in interglacial periods and the period around the MIS 18. Published endmember data of clay minerals and Sr-Nd isotopic composition for possible source sediments of the WAIS are from previous studies (Hillenbrand, 2001, Pant et al., 2013, Ehrmann et al., 2005, Diekmann et al., 2004, Setti et al., 2004, Ehrmann et al., 2011, Hillenbrand et al., 2003) and (Simões Pereira et al., 2018, Blakowski et al., 2016, Adams et al., 2004, Adams, 1987, Wever et al., 1994, Scarrow et al., 1998, Riley et al., 2001, Wever and Storey, 1992, Curtis et al., 1999, Futa and Lemasurier, 1983, Hart et al., 1997), respectively. Red shading represents a mixture of icebergs from the RSE and ASE; blue shading represents icebergs mainly from the ASE, and orange shading represents the mixture of icebergs from north Victoria Land and the ASE.

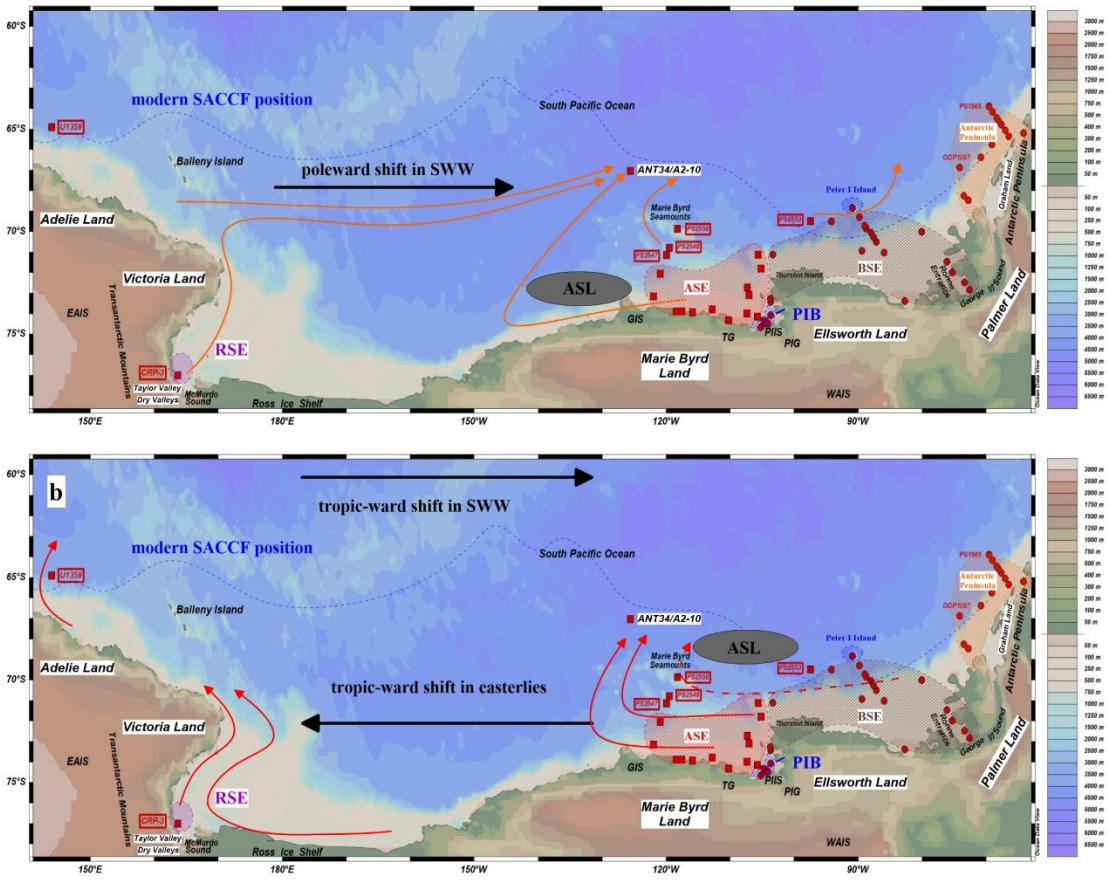

Figure 5. Systematic diagram of iceberg trajectory at the IRD peak interval in the interglacial period, low IRD content interval in the glacial period, and the period around MIS 18.

a, iceberg trajectory at the IRD peak interval in the interglacial period and the period around MIS 18; b, iceberg trajectory at the low IRD content interval in the glacial period. ASL: Amundsen Sea Low-pressure system. Red, blue, brown, and orange shade indicate the ASE, PIB, BSE, and Antarctic Peninsula, respectively. Orange lines indicate the iceberg's trajectory in the IRD peak interval in the interglacial period, which is modified from (Gladstone et al., 2001, England et al., 2020, Tournadre et al., 2016). Red lines indicate the iceberg's trajectory in the low IRD content interval in the glacial period and the black arrow represents the poleward/tropicward shift of SWW and tropicward shift of easterlies.

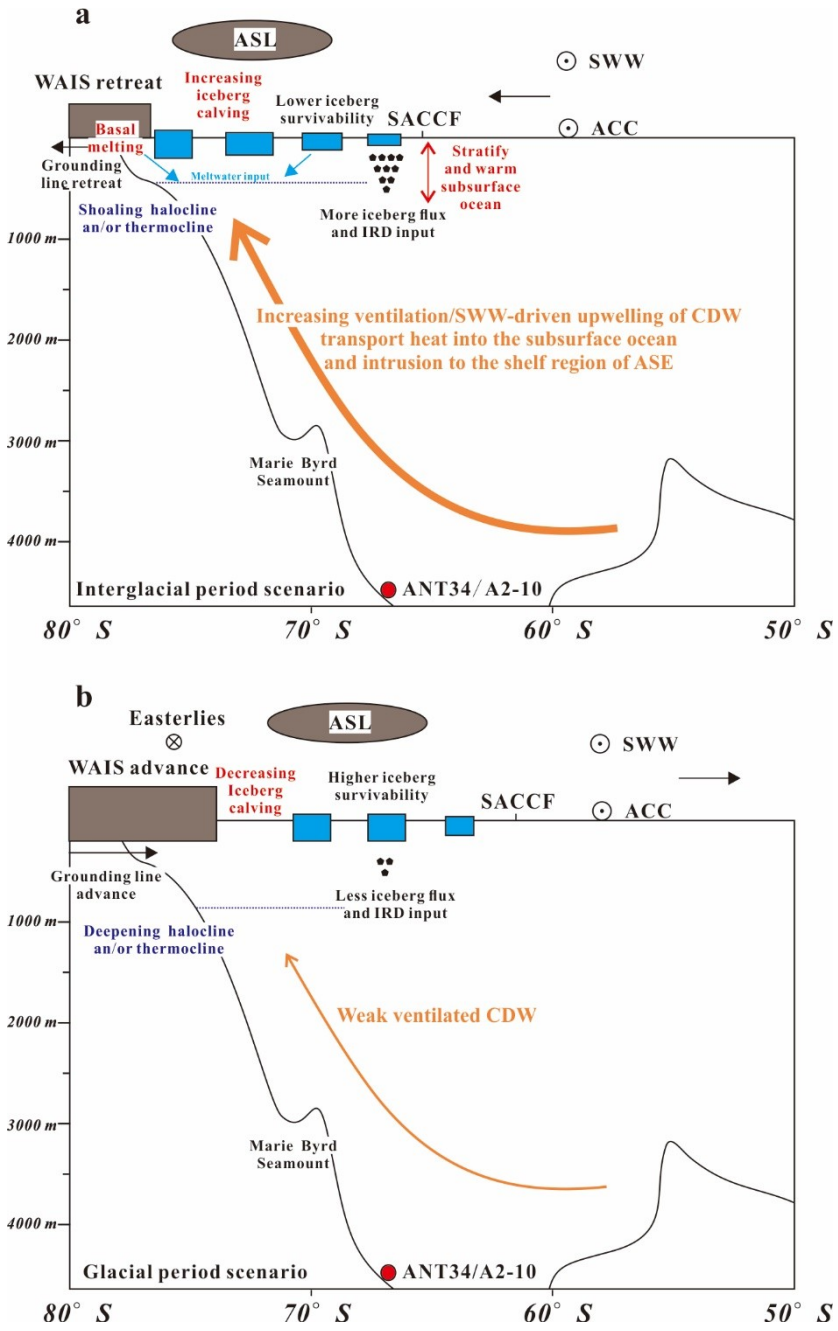

Figure 6. Systematic diagram of ocean-driven positive feedback processes at the IRD peak interval in the a, interglacial period scenario and b, glacial period scenario.

Declaration of competing interest

The authors declare that they have no known competing financial interests or personal relationships that could have influenced the work reported in this paper.

Acknowledgments: We thank the 34th Chinese Antarctic Expedition cruise members and the Chinese Arctic and Antarctic Administration for retrieving the sediment core. Age model data of core ANT34/A2-10 are currently being archived in PANGAEA and will be publicly available upon acceptance. For review purposes, the data are uploaded as supporting information. This work was supported by Impact and Response of Antarctic Seas to Climate Change (IRASCC2020-2022-01-03-02 and 02-03), Basic Scientific Fund for National Public Research Institutes of China (Grant no. 2019Q09, 2019S04, and 2017Y07), the National Natural Science Foundation of China (Grant no. 41976080, 42076232 and 41406220), the Taishan Scholars Project Funding (Grant No ts20190963)

References

Adams, C. J. (1987), Geochronology of granite terranes in the Ford Ranges, Marie Byrd Land, West Antarctica. *New Zealand Journal of Geology and Geophysics*. 30 (1), 51-72. doi:10.1080/00288306.1987.10422193

Adams, C. J., Seward, D. & Weaver, S. D. (2004), Geochronology of Cretaceous granites and metasedimentary basement on Edward VII Peninsula, Marie Byrd Land, West Antarctica. *Antarctic Science*. 7 (3), 265-276. doi:10.1017/s095410209500037x

Adusumilli, S., Fricker, H. A., Medley, B., Padman, L. & Siegfried, M. R. (2020), Interannual variations in meltwater input to the Southern Ocean from Antarctic ice shelves. *Nature Geoscience*. 13 (9), 616-620. doi:10.1038/s41561-020-0616-z

Anderson, R. F., Ali, S., Bradtmiller, L. I., Nielsen, S. H., Fleisher, M. Q., Anderson, B. E. & Burckle, L. H. (2009), Wind-driven upwelling in the Southern Ocean and the deglacial rise in atmospheric CO_2. *Science*. 323 (5920), 1443-8. doi:10.1126/science.1167441

Baines, P. G. & Fraedrich, K. (1988), Topographic Effects on the Mean Tropospheric Flow Patterns around Antarctica. *Journal of the Atmospheric Sciences*. 46 (22), 3401-3415. doi:10.1175/1520-0469(1989)046

Bell, R. E. (2008), The role of subglacial water in ice-sheet mass balance. *Nature Geoscience*. 1 (5), 297-304. doi:10.1038/ngeo186

Benz, V., Esper, O., Gersonde, R., Lamy, F. & Tiedemann, R. (2016), Last Glacial Maximum sea surface temperature and sea-ice extent in the Pacific sector of the Southern Ocean. *Quaternary Science Reviews*. 146, 216-237.

704 doi:10.1016/j.quascirev.2016.06.006
705 Bigg, G. R. (2020), The impact of icebergs of sub-Antarctic origin on Southern Ocean
706 ice-rafted debris distributions. *Quaternary Science Reviews*. 232
707 doi:10.1016/j.quascirev.2020.106204
708 Biscaye, P. E. (1965), Mineralogy and Sedimentation of Recent Deep-Sea Clay in the
709 Atlantic Ocean and Adjacent Seas and Oceans. *Geological Society of America*
710 *Bulletin*. 76, 803-832.
711 Blakowski, M. A., Aciego, S. M., Delmonte, B., Baroni, C., Salvatore, M. C. & Sims,
712 K. W. W. (2016), A Sr-Nd-Hf isotope characterization of dust source areas in
713 Victoria Land and the McMurdo Sound sector of Antarctica. *Quaternary*
714 *Science Reviews*. 141, 26-37. doi:10.1016/j.quascirev.2016.03.023
715 Bronselaer, B., Winton, M., Griffies, S. M., Hurlin, W. J., Rodgers, K. B., Sergienko,
716 O. V., Stouffer, R. J. & Russell, J. L. (2018), Change in future climate due to
717 Antarctic meltwater. *Nature*. 564 (7734), 53-58. doi:10.1038/s41586-018-
718 0712-z
719 Budillon, G. & Spezie, G. (2004), Thermohaline structure and variability in the Terra
720 Nova Bay polynya, Ross Sea. *Antarctic Science*. 12 (4), 493-508. doi:10.1017/
721 s0954102000000572
722 Caburlotto, A., Lucchi, R. G., De Santis, L., Macrì, P. & Tolotti, R. (2009),
723 Sedimentary processes on the Wilkes Land continental rise reflect changes in
724 glacial dynamic and bottom water flow. *International Journal of Earth*
725 *Sciences*. 99 (4), 909-926. doi:10.1007/s00531-009-0422-8
726 Caniupán, M., Lamy, F., Lange, C. B., Kaiser, J., Arz, H., Kilian, R., Baeza Urrea, O.,
727 Aracena, C., Hebbeln, D., Kissel, C., Laj, C., Mollenhauer, G. & Tiedemann,
728 R. (2011), Millennial-scale sea surface temperature and Patagonian Ice Sheet
729 changes off southernmost Chile (53°S) over the past ~60 kyr.
730 *Paleoceanography*. 26 (3), n/a-n/a. doi:10.1029/2010pa002049
731 Ceccaroni, L., Frank, M., Frignani, M., Langone, L., Ravaioli, M. & Mangini, A.
732 (1998), Late Quaternary fluctuations of biogenic component fluxes on the
733 continental slope of the Ross Sea, Antarctica. *Journal of Marine Systems*. 17
734 (1-4), 515-525. doi:10.1016/s0924-7963(98)00061-x
735 Charles, C. D., Pahnke, K., Zahn, R., Mortyn, P. G., Ninnemann, U. & Hodell, D. A.
736 (2010), Millennial scale evolution of the Southern Ocean chemical divide.
737 *Quaternary Science Reviews*. 29 (3-4), 399-409.
738 doi:10.1016/j.quascirev.2009.09.021
739 Conway, H., Hall, B. L., Denton, G. H., Gades, A. M. & Waddington, E. D. (1999),
740 Past and Future Grounding-Line Retreat of the West Antarctic Ice Sheet.
741 *Science*. 286 (5438), 280-283. doi:10.1126/science.286.5438.280
742 Curtis, M. L., Leat, P. T., Riley, T. R., Storey, B. C., Millar, I. L. & Randall, D. E.
743 (1999), Middle Cambrian rift-related volcanism in the Ellsworth Mountains,
744 Antarctica: tectonic implications for the palaeo-Pacific margin of Gondwana.
745 *Tectonophysics*. 304 (4), 275-299. doi:10.1016/s0040-1951(99)00033-5
746 Das, I., Padman, L., Bell, R. E., Fricker, H. A., Tinto, K. J., Hulbe, C. L., Siddoway,
747 C. S., Dhakal, T., Frearson, N. P., Mosbeux, C., Cordero, S. I. & Siegfried, M.

748 R. (2020), Multidecadal Basal Melt Rates and Structure of the Ross Ice Shelf,
749 Antarctica, Using Airborne Ice Penetrating Radar. *Journal of Geophysical*
750 *Research: Earth Surface*. 125 (3)doi:10.1029/2019jf005241
751 Davis, P. E. D., Jenkins, A., Nicholls, K. W., Brennan, P. V., Abrahamsen, E. P.,
752 Heywood, K. J., Dutrieux, P., Cho, K. H. & Kim, T. W. (2018), Variability in
753 Basal Melting Beneath Pine Island Ice Shelf on Weekly to Monthly
754 Timescales. *Journal of Geophysical Research-Oceans*. 123 (11), 8655-8669.
755 doi:10.1029/2018jc014464
756 Diekmann, B., Kuhn, G., Gersonde, R. & Mackensen, A. (2004), Middle Eocene to
757 early Miocene environmental changes in the sub-Antarctic Southern Ocean:
758 evidence from biogenic and terrigenous depositional patterns at ODP Site
759 1090. *Global and Planetary Change*. 40 (3-4), 295-313.
760 doi:10.1016/j.gloplacha.2003.09.001
761 Dinniman, M. S., Klinck, J. M. & Hofmann, E. E. (2012), Sensitivity of Circumpolar
762 Deep Water Transport and Ice Shelf Basal Melt along the West Antarctic
763 Peninsula to Changes in the Winds. *Journal of Climate*. 25 (14), 4799-4816.
764 doi:10.1175/Jcli-D-11-00307.1
765 Ehrmann, W. (1998), Implications of late Eocene to early Miocene clay mineral
766 assemblages in McMurdo Sound (Ross Sea, Antarctica) on paleoclimate and
767 ice dynamics. *Palaeogeography, Palaeoclimatology, Palaeoecology*. 139 (3-
768 4), 213-231. doi:10.1016/s0031-0182(97)00138-7
769 Ehrmann, W., Hillenbrand, C. D., Smith, J. A., Graham, A. G. C., Kuhn, G. & Larter,
770 R. D. (2011), Provenance changes between recent and glacial-time sediments
771 in the Amundsen Sea embayment, West Antarctica: clay mineral assemblage
772 evidence. *Antarctic Science*. 23 (5), 471-486.
773 doi:10.1017/S0954102011000320
774 Ehrmann, W., Setti, M. & Marinoni, L. (2005), Clay minerals in Cenozoic sediments
775 off Cape Roberts (McMurdo Sound, Antarctica) reveal palaeoclimatic history.
776 *Palaeogeography Palaeoclimatology Palaeoecology*. 229 (3), 187-211.
777 doi:10.1016/j.palaeo.2005.06.022
778 Ehrmann, W. U., Grobe, H. & Fütterer, D. K. 1991. Late Miocene to Holocene Glacial
779 History of East Antarctica as Revealed by Sediments from Sites 745 and 746.
780 *Proceedings of the Ocean Drilling Program, 119 Scientific Results.*
781 Ehrmann, W. U., Melles, M., Kuhn, G. & Grobe, H. (1992), Significance of clay
782 mineral assemblages in the Antarctic Ocean. *Marine Geology*. 107 (4), 249-
783 273. doi:10.1016/0025-3227(92)90075-s
784 England, M. R., Wagner, T. J. W. & Eisenman, I. (2020), Modeling the breakup of
785 tabular icebergs. *Science Advances*. 6 (51)doi:10.1126/sciadv.abd1273
786 Fogwill, C. J., Phipps, S. J., Turney, C. S. M. & Golledge, N. R. (2015), Sensitivity of
787 the Southern Ocean to enhanced regional Antarctic ice sheet meltwater input.
788 *Earths Future*. 3 (10), 317-329. doi:10.1002/2015ef000306
789 Futa, K. & Lemasurier, W. E. (1983), Nd and Sr Isotopic Studies on Cenozoic Mafic
790 Lavas from West Antarctica - Another Source for Continental Alkali Basalts.
791 *Contributions to Mineralogy and Petrology*. 83 (1-2), 38-44.

792 doi:10.1007/Bf00373077
793 Gingele, F. X., De Deckker, P. & Hillenbrand, C.-D. (2001), Clay mineral distribution
794 in surface sediments between Indonesia and NW Australia — source and
795 transport by ocean currents. *Marine Geology*. 179 (3-4), 135-146. doi:10.1016/
796 s0025-3227(01)00194-3
797 Gingele, F. X., Müller, P. M. & Schneider, R. R. (1998), Orbital forcing of freshwater
798 input in the Zaire Fan area—clay mineral evidence from the last 200 kyr.
799 *Palaeogeography, Palaeoclimatology, Palaeoecology*. 138 (1-4), 17-26.
800 doi:10.1016/s0031-0182(97)00121-1
801 Gladstone, R. M., Bigg, G. R. & Nicholls, K. W. (2001), Iceberg trajectory modeling
802 and meltwater injection in the Southern Ocean. *Journal of Geophysical*
803 *Research: Oceans*. 106 (C9), 19903-19915. doi:10.1029/2000jc000347
804 Golledge, N. R., Keller, E. D., Gomez, N., Naughten, K. A., Bernales, J., Trusel, L. D.
805 & Edwards, T. L. (2019), Global environmental consequences of twenty-first-
806 century ice-sheet melt. *Nature*. 566 (7742), 65-72. doi:10.1038/s41586-019-
807 0889-9
808 Graly, J. A., Licht, K. J., Bader, N. A. & Bish, D. L. (2020), Chemical weathering
809 signatures from Mt. Achernar Moraine, Central Transantarctic Mountains I:
810 Subglacial sediments compared with underlying rock. *Geochimica Et*
811 *Cosmochimica Acta*. 283, 149-166. doi:10.1016/j.gca.2020.06.005
812 Grinsted, A., Moore, J. C. & Jevrejeva, S. (2004), Application of the cross wavelet
813 transform and wavelet coherence to geophysical time series. *Nonlinear*
814 *Processes in Geophysics*. 11 (5/6), 561-566. doi:10.5194/npg-11-561-2004
815 Hall, I. R., McCave, I. N., Shackleton, N. J., Weedon, G. P. & Harris, S. E. (2001),
816 Intensified deep Pacific inflow and ventilation in Pleistocene glacial times.
817 *Nature*. 412 (6849), 809-12. doi:10.1038/35090552
818 Hammer, Ø. & Harper, D. A. (2008). *Paleontological data analysis*: John Wiley &
819 Sons.
820 Hansen, J., Sato, M., Hearty, P., Ruedy, R., Kelley, M., Masson-Delmotte, V., Russell,
821 G., Tselioudis, G., Cao, J., Rignot, E., Velicogna, I., Tormey, B., Donovan, B.,
822 Kandiano, E., von Schuckmann, K., Kharecha, P., Legrande, A. N., Bauer, M.
823 & Lo, K.-W. (2016), Ice melt, sea level rise and superstorms: evidence from
824 paleoclimate data, climate modeling, and modern observations that 2 °C
825 global warming could be dangerous. *Atmospheric Chemistry and Physics*. 16
826 (6), 3761-3812. doi:10.5194/acp-16-3761-2016
827 Hart, S. R., Blusztajn, J., LeMasurier, W. E. & Rex, D. C. (1997), Hobbs Coast
828 Cenozoic volcanism: Implications for the West Antarctic rift system. *Chemical*
829 *Geology*. 139 (1-4), 223-248. doi:10.1016/S0009-2541(97)00037-5
830 Hillenbrand, C.-D., Grobe, H., Diekmann, B., Kuhn, G. & Fütterer, D. K. (2003),
831 Distribution of clay minerals and proxies for productivity in surface sediments
832 of the Bellingshausen and Amundsen seas (West Antarctica) – Relation to
833 modern environmental conditions. *Marine Geology*. 193 (3-4), 253-271.
834 doi:10.1016/s0025-3227(02)00659-x
835 Hillenbrand, C. D. & Ehrmann, W. (2005), Late Neogene to Quaternary

836 environmental changes in the Antarctic Peninsula region: evidence from drift
837 sediments. *Global and Planetary Change*. 45 (1-3), 165-191.
838 doi:10.1016/j.gloplacha.2004.09.006
839 Hillenbrand, C. D., Ehrmann, W., Larter, R. D., Benetti, S., Dowdeswell, J. A.,
840 Cofaigh, C. O., Graham, A. G. C. & Grobe, H. (2009a), Clay mineral
841 provenance of sediments in the southern Bellingshausen Sea reveals drainage
842 changes of the West Antarctic Ice Sheet during the Late Quaternary. *Marine*
843 *Geology*. 265 (1-2), 1-18. doi:10.1016/j.margeo.2009.06.009
844 Hillenbrand, C. D., Kuhn, G. & Frederichs, T. (2009b), Record of a Mid-Pleistocene
845 depositional anomaly in West Antarctic continental margin sediments: an
846 indicator for ice-sheet collapse? *Quaternary Science Reviews*. 28 (13-14),
847 1147-1159. doi:10.1016/j.quascirev.2008.12.010
848 Hillenbrand, E. (2001), Distribution of clay minerals in drift sediments on the
849 continental rise west of the antarctic peninsula, odp leg 178, sites 1095 and
850 1096. *Proceedings of the Ocean Drilling Program: Scientific Results*. 178, 1-
851 29.
852 Hiscock, M. R. 2004. The regulation of primary productivity in the Southern Ocean.
853 Ph.D, Duke University.
854 Hodell, D. A. & Venz-Curtis, K. A. (2006), Late Neogene history of deepwater
855 ventilation in the Southern Ocean. *Geochemistry Geophysics Geosystems*. 7
856 (9), n/a-n/a. doi:10.1029/2005GC001211
857 Hodell, D. A., Venz, K. A., Charles, C. D. & Ninnemann, U. S. (2003), Pleistocene
858 vertical carbon isotope and carbonate gradients in the South Atlantic sector of
859 the Southern Ocean. *Geochemistry Geophysics Geosystems*. 4 (1), 1-19.
860 doi:10.1029/2002GC000367
861 Hosking, J. S., Orr, A., Bracegirdle, T. J. & Turner, J. (2016), Future circulation
862 changes off West Antarctica: Sensitivity of the Amundsen Sea Low to
863 projected anthropogenic forcing. *Geophysical Research Letters*. 43 (1), 367-
864 376. doi:10.1002/2015gl067143
865 Huybers, P. (2007), Glacial variability over the last two million years: an extended
866 depth-derived agemodel, continuous obliquity pacing, and the Pleistocene
867 progression. *Quaternary Science Reviews*. 26 (1-2), 37-55.
868 doi:10.1016/j.quascirev.2006.07.013
869 Huybers, P. & Wunsch, C. (2005), Obliquity pacing of the late Pleistocene glacial
870 terminations. *Nature*. 434 (7032), 491-4. doi:10.1038/nature03401
871 Huybrechts, P. (2002), Sea-level changes at the LGM fromice-dynamic
872 reconstructions of the Greenland and Antarctic ice sheets during the glacial
873 cycles. *Quaternary Science Reviews*. 21, 203-231.
874 Jacobs, S., Jenkins, A., Hellmer, H., Giulivi, C., Nitsche, F., Huber, B. & Guerrero, R.
875 (2012), The Amundsen Sea and the Antarctic Ice Sheet. *Oceanography*. 25 (3),
876 154-163. doi:10.5670/oceanog.2012.90
877 Jacobs, S. S. & Comiso, J. C. (1997), Climate Variability in the Amundsen and
878 Bellingshausen Seas. *Journal of Climate*. 10 (4), 697-709. doi:10.1175/1520-
879 0442(1997)0102.0.CO;2

880 Jacobs, S. S., Fairbanks, R. G., & Horibe, Y. . (1985), Origin and evolution of water
881 masses near the Antarctic continental margin: Evidence from $H_2{}^{18}O/H_2{}^{16}O$
882 ratios in seawater. *Oceanology of the Antarctic continental shelf*. 43 (59-
883 85)doi:10.1029/AR043p0059
884 Jacobs, S. S., Hellmer, H. H. & Jenkins, A. (1996), Antarctic ice sheet melting in the
885 Southeast Pacific. *Geophysical Research Letters*. 23 (9), 957-960.
886 doi:10.1029/96gl00723
887 Jacobs, S. S., Helmer, H. H., Doake, C. S. M., Jenkins, A. & Frolich, R. M. (2017),
888 Melting of ice shelves and the mass balance of Antarctica. *Journal of*
889 *Glaciology*. 38 (130), 375-387. doi:10.3189/s0022143000002252
890 Jacobs, S. S., Jenkins, A., Giulivi, C. F. & Dutrieux, P. (2011), Stronger ocean
891 circulation and increased melting under Pine Island Glacier ice shelf. *Nature*
892 *Geoscience*. 4 (8), 519-523. doi:10.1038/Ngeo1188
893 Jones, R. S., Gudmundsson, G. H., Mackintosh, A. N., McCormack, F. S. &
894 Whitmore, R. J. (2021), Ocean−Driven and Topography−Controlled Nonlinear
895 Glacier Retreat During the Holocene: Southwestern Ross Sea, Antarctica.
896 *Geophysical Research Letters*. 48 (5)doi:10.1029/2020gl091454
897 Joughin, I. & Alley, R. B. (2011), Stability of the West Antarctic ice sheet in a
898 warming world. *Nature Geoscience*. 4 (8), 506-513. doi:10.1038/Ngeo1194
899 Joughin, I., Smith, B. E. & Medley, B. (2014), Marine ice sheet collapse potentially
900 under way for the Thwaites Glacier Basin, West Antarctica. *Science*. 344
901 (6185), 735-8. doi:10.1126/science.1249055
902 Jouzel, J., Masson-Delmotte, V., Cattani, O., Dreyfus, G., Falourd, S., Hoffmann, G.,
903 Minster, B., Nouet, J., Barnola, J. M., Chappellaz, J., Fischer, H., Gallet, J. C.,
904 Johnsen, S., Leuenberger, M., Loulergue, L., Luethi, D., Oerter, H., Parrenin,
905 F., Raisbeck, G., Raynaud, D., Schilt, A., Schwander, J., Selmo, E., Souchez,
906 R., Spahni, R., Stauffer, B., Steffensen, J. P., Stenni, B., Stocker, T. F., Tison, J.
907 L., Werner, M. & Wolff, E. W. (2007), Orbital and millennial Antarctic climate
908 variability over the past 800,000 years. *Science*. 317 (5839), 793-6.
909 doi:10.1126/science.1141038
910 Kanfoush, S. L., Hodell, D. A., Charles, C. D., Guilderson, T. P., Mortyn, P. G. &
911 Ninnemann, U. S. (2000), Millennial-scale instability of the antarctic ice sheet
912 during the last glaciation. *Science*. 288 (5472), 1815-8.
913 doi:10.1126/science.288.5472.1815
914 Konfirst, M. A., Scherer, R. P., Hillenbrand, C.-D. & Kuhn, G. (2012), A marine
915 diatom record from the Amundsen Sea — Insights into oceanographic and
916 climatic response to the Mid-Pleistocene Transition in the West Antarctic
917 sector of the Southern Ocean. *Marine Micropaleontology*. 92-93, 40-51.
918 doi:10.1016/j.marmicro.2012.05.001
919 Krylov, A. A., Andreeva, I. A., Vogt, C., Backman, J., Krupskaya, V. V., Grikurov, G.
920 E., Moran, K. & Shoji, H. (2008), A shift in heavy and clay mineral
921 provenance indicates a middle Miocene onset of a perennial sea ice cover in
922 the Arctic Ocean. *Paleoceanography*. 23 (1), n/a-n/a.
923 doi:10.1029/2007pa001497

924 Larour, E., Seroussi, H., Adhikari, S., Ivins, E., Caron, L., Morlighem, M. & Schlegel,
925 N. (2019), Slowdown in Antarctic mass loss from solid Earth and sea-level
926 feedbacks. *Science*. 364 (6444)doi:10.1126/science.aav7908
927 Laskar, J., Robutel, P., Joutel, F., Gastineau, M., Correia, A. C. M. & Levrard, B.
928 (2004), A long-term numerical solution for the insolation quantities
929 of the Earth. *Astronomy & Astrophysics*. 428 (1), 261-285. doi:10.1051/0004-
930 6361:20041335
931 Lear, C. H., Rosenthal, Y., Coxall, H. K. & Wilson, P. A. (2004), Late Eocene to early
932 Miocene ice sheet dynamics and the global carbon cycle. *Paleoceanography*.
933 19 (4), n/a-n/a. doi:10.1029/2004pa001039
934 Levy, R. H., Meyers, S. R., Naish, T. R., Golledge, N. R., McKay, R. M., Crampton, J.
935 S., DeConto, R. M., De Santis, L., Florindo, F., Gasson, E. G. W., Harwood,
936 D. M., Luyendyk, B. P., Powell, R. D., Clowes, C. & Kulhanek, D. K. (2019),
937 Antarctic ice-sheet sensitivity to obliquity forcing enhanced through ocean
938 connections. *Nature Geoscience*. 12 (2), 132-+. doi:10.1038/s41561-018-
939 0284-4
940 Li, M. S., Hinnov, L. & Kump, L. (2019), Acycle: Time-series analysis software for
941 paleoclimate research and education. *Computers & Geosciences*. 127, 12-22.
942 doi:10.1016/j.cageo.2019.02.011
943 Lindgren, A., Hugelius, G. & Kuhry, P. (2018), Extensive loss of past permafrost
944 carbon but a net accumulation into present-day soils. *Nature*. 560 (7717), 219-
945 222. doi:10.1038/s41586-018-0371-0
946 Liu, Y., Moore, J. C., Cheng, X., Gladstone, R. M., Bassis, J. N., Liu, H., Wen, J. &
947 Hui, F. (2015), Ocean-driven thinning enhances iceberg calving and retreat of
948 Antarctic ice shelves. *Proc Natl Acad Sci U S A*. 112 (11), 3263-8.
949 doi:10.1073/pnas.1415137112
950 Lovenduski, N. S. (2005), Impact of the Southern Annular Mode on Southern Ocean
951 circulation and biology. *Geophysical Research Letters*. 32
952 (11)doi:10.1029/2005gl022727
953 Lowe, A. & Anderson, J. (2002), Reconstruction of the West Antarctic ice sheet in
954 Pine Island Bay during the Last Glacial Maximum and its subsequent retreat
955 history. *Quaternary Science Reviews*. 21 (16-17), 1879-1897.
956 doi:10.1016/s0277-3791(02)00006-9
957 McCulloch, R. D., Blaikie, J., Jacob, B., Mansilla, C. A., Morello, F., De Pol-Holz, R.,
958 San Román, M., Tisdall, E. & Torres, J. (2020), Late glacial and Holocene
959 climate variability, southernmost Patagonia. *Quaternary Science Reviews*. 229
960 doi:10.1016/j.quascirev.2019.106131
961 Members, W. D. P. (2013), Onset of deglacial warming in West Antarctica driven by
962 local orbital forcing. *Nature*. 500 (7463), 440-4. doi:10.1038/nature12376
963 Menviel, L., Timmermann, A., Timm, O. E. & Mouchet, A. (2010), Climate and
964 biogeochemical response to a rapid melting of the West Antarctic Ice Sheet
965 during interglacials and implications for future climate. *Paleoceanography*. 25
966 (4), n/a-n/a. doi:10.1029/2009pa001892
967 Mix, A. C., Pisias, N. G., Rugh, W., Wilson, J. & Hagelberg, T. K. J. P. o. t. O. D. P. S.

R. (1995), 17. Benthic foraminifer stable isotope record from Site 849 (0–5 Ma): Local and global climate changes. 138

Nakayama, Y., Menemenlis, D., Zhang, H., Schodlok, M. & Rignot, E. (2018), Origin of Circumpolar Deep Water intruding onto the Amundsen and Bellingshausen Sea continental shelves. *Nature Communications*. 9 (1), 3403. doi:10.1038/s41467-018-05813-1

Nerem, R. S., Beckley, B. D., Fasullo, J. T., Hamlington, B. D., Masters, D. & Mitchum, G. T. (2018), Climate-change-driven accelerated sea-level rise detected in the altimeter era. *Proc Natl Acad Sci U S A*. 115 (9), 2022-2025. doi:10.1073/pnas.1717312115

Nielsen, S. H. & Hodell, D. A. (2007), Antarctic Ice-Rafted Detritus (IRD) in the South Atlantic: Indicators of Iceshelf Dynamics or Ocean Surface Conditions? *Antarctic Ice-Rafted Detritus (IRD) in the South Atlantic: Indicators of Iceshelf Dynamics or Ocean Surface Conditions?* 2007 (1047srp020)doi:10.3133/of2007-1047.srp020

Nielsen, S. H. H., Hodell, D. A., Kamenov, G., Guilderson, T. & Perfit, M. R. (2007), Origin and significance of ice-rafted detritus in the Atlantic sector of the Southern Ocean. *Geochemistry Geophysics Geosystems*. 8 (12), n/a-n/a. doi:10.1029/2007GC001618

Oliveira, D., Desprat, S., Yin, Q., Rodrigues, T., Naughton, F., Trigo, R. M., Su, Q., Grimalt, J. O., Alonso-Garcia, M., Voelker, A. H. L., Abrantes, F. & Sánchez Goñi, M. F. (2020), Combination of insolation and ice-sheet forcing drive enhanced humidity in northern subtropical regions during MIS 13. *Quaternary Science Reviews*. 247 doi:10.1016/j.quascirev.2020.106573

Orsi, A. H., Whitworth, T. & Nowlin, W. D. (1995), On the Meridional Extent and Fronts of the Antarctic Circumpolar Current. *Deep-Sea Research Part I-Oceanographic Research Papers*. 42 (5), 641-673. doi:10.1016/0967-0637(95)00021-W

Pant, N. C., Biswas, P., Shrivastava, P. K., Bhattacharya, S., Verma, K. & Pandey, M. (2013). *Provenance of Pleistocene sediments from Site U1359 of the Wilkes Land IODP Leg 318 – evidence for multiple sourcing from the East Antarctic Craton and Ross Orogen* (Vol. 381). Geological Society, London.

Patterson, M. O., McKay, R., Naish, T., Escutia, C., Jimenez-Espejo, F. J., Raymo, M. E., Meyers, S. R., Tauxe, L., Brinkhuis, H. & Scientists, I. E. (2014), Orbital forcing of the East Antarctic ice sheet during the Pliocene and Early Pleistocene. *Nature Geoscience*. 7 (11), 841-847. doi:10.1038/Ngeo2273

Pattyn, F. & Morlighem, M. (2020), The uncertain future of the Antarctic Ice Sheet. *Science*. 367 (6484), 1331-1335. doi:10.1126/science.aaz5487

Perez, L. F., Martos, Y. M., Garcia, M., Weber, M. E., Raymo, M. E., Williams, T., Bohoyo, F., Armbrecht, L., Bailey, I., Brachfeld, S., Gluder, A., Guitard, M., Gutjahr, M., Hemming, S., Hernandez-Almeida, I., Hoem, F. S., Kato, Y., O'Connell, S., Peck, V. L., Reilly, B., Ronge, T. A., Tauxe, L., Warnock, J., Zheng, X. F. & Scientists, I. E. (2021), Miocene to present oceanographic variability in the Scotia Sea and Antarctic ice sheets dynamics: Insight from

revised seismic-stratigraphy following IODP Expedition 382. *Earth and Planetary Science Letters*. 553 doi:10.1016/j.epsl.2020.1166570012-821X

Petschick, R., Kuhn, G. & Gingele, F. (1996), Clay mineral distribution in surface sediments of the South Atlantic: sources, transport, and relation to oceanography. *Marine Geology*. 130 (3-4), 203-229. doi:10.1016/0025-3227(95)00148-4

Phillips, T., Turner, J., Marshall, G. J., Orr, A. & Hosking, J. S. (2013), The Influence of the Amundsen–Bellingshausen Seas Low on the Climate of West Antarctica and Its Representation in Coupled Climate Model Simulations. *Journal of Climate*. 26 (17), 6633-6648. doi:10.1175/jcli-d-12-00813.1

Pollard, D. & DeConto, R. M. (2009), Modelling West Antarctic ice sheet growth and collapse through the past five million years. *Nature*. 458 (7236), 329-32. doi:10.1038/nature07809

Presti, M., Barbara, L., Denis, D., Schmidt, S., De Santis, L. & Crosta, X. (2011), Sediment delivery and depositional patterns off Adélie Land (East Antarctica) in relation to late Quaternary climatic cycles. *Marine Geology*. 284 (1-4), 96-113. doi:10.1016/j.margeo.2011.03.012

Pritchard, H. D., Ligtenberg, S. R., Fricker, H. A., Vaughan, D. G., van den Broeke, M. R. & Padman, L. (2012), Antarctic ice-sheet loss driven by basal melting of ice shelves. *Nature*. 484 (7395), 502-5. doi:10.1038/nature10968

Richardson, G. (2005), Short-term climate response to a freshwater pulse in the Southern Ocean. *Geophysical Research Letters*. 32 (3)doi:10.1029/2004gl021586

Rignot, E., Jacobs, S., Mouginot, J. & Scheuchl, B. (2013), Ice-shelf melting around Antarctica. *Science*. 341 (6143), 266-70. doi:10.1126/science.1235798

Rignot, E. & Jacobs, S. S. (2002), Rapid bottom melting widespread near Antarctic Ice Sheet grounding lines. *Science*. 296 (5575), 2020-3. doi:10.1126/science.1070942

Rignot, E., Mouginot, J., Morlighem, M., Seroussi, H. & Scheuchl, B. (2014), Widespread, rapid grounding line retreat of Pine Island, Thwaites, Smith, and Kohler glaciers, West Antarctica, from 1992 to 2011. *Geophysical Research Letters*. 41 (10), 3502-3509. doi:10.1002/2014gl060140

Rignot, E., Mouginot, J., Scheuchl, B., van den Broeke, M., van Wessem, M. J. & Morlighem, M. (2019), Four decades of Antarctic Ice Sheet mass balance from 1979-2017. *Proc Natl Acad Sci U S A*. 116 (4), 1095-1103. doi:10.1073/pnas.1812883116

Riley, T. R., Leat, P. T., Pankhurst, R. J. & Harris, C. (2001), Origins of Large Volume Rhyolitic Volcanism in the Antarctic Peninsula and Patagonia by Crustal Melting. *Journal of Petrology*. 42 (6), 1043-1065. doi:10.1093/petrology/42.6.1043

Scarrow, J. H., Leat, P. T., Wareham, C. D., Millar, I. L. J. C. t. M. & Petrology. (1998), Geochemistry of mafic dykes in the Antarctic Peninsula continental-margin batholith: a record of arc evolution. 131 (2-3), 289-305.

Schmidtko, S., Heywood, K. J., Thompson, A. F. & Aoki, S. (2014), Multidecadal

warming of Antarctic waters. *Science*. 346 (6214), 1227-31. doi:10.1126/science.1256117

Sen Gupta, A. & McNeil, B. 2012. Variability and Change in the Ocean. *The Future of the World's Climate.*

Setti, M., Marinoni, L. & Lopez-Galindo, A. (2004), Mineralogical and geochemical characteristics (major, minor, trace elements and REE) of detrital and authigenic clay minerals in a Cenozoic sequence from Ross Sea, Antarctica. *Clay Minerals*. 39 (4), 405-421. doi:10.1180/000985503540143

Shepherd, A., Fricker, H. A. & Farrell, S. L. (2018), Trends and connections across the Antarctic cryosphere. *Nature*. 558 (7709), 223-232. doi:10.1038/s41586-018-0171-6

Silva, T. A. M., Bigg, G. R. & Nicholls, K. W. (2006), Contribution of giant icebergs to the Southern Ocean freshwater flux. *Journal of Geophysical Research*. 111 (C3)doi:10.1029/2004jc002843

Simões Pereira, P., van de Flierdt, T., Hemming, S. R., Hammond, S. J., Kuhn, G., Brachfeld, S., Doherty, C. & Hillenbrand, C.-D. (2018), Geochemical fingerprints of glacially eroded bedrock from West Antarctica: Detrital thermochronology, radiogenic isotope systematics and trace element geochemistry in Late Holocene glacial-marine sediments. *Earth-Science Reviews*. 182, 204-232. doi:10.1016/j.earscirev.2018.04.011

Smith, W. O., Shields, A. R., Peloquin, J. A., Catalano, G., Tozzi, S., Dinniman, M. S. & Asper, V. A. (2006), Interannual variations in nutrients, net community production, and biogeochemical cycles in the Ross Sea. *Deep-Sea Research Part Ii-Topical Studies in Oceanography*. 53 (8-10), 815-833. doi:10.1016/j.dsr2.2006.02.014

Starr, A., Hall, I. R., Barker, S., Rackow, T., Zhang, X., Hemming, S. R., van der Lubbe, H. J. L., Knorr, G., Berke, M. A., Bigg, G. R., Cartagena-Sierra, A., Jimenez-Espejo, F. J., Gong, X., Gruetzner, J., Lathika, N., LeVay, L. J., Robinson, R. S., Ziegler, M. & Expedition 361 Science, P. (2021), Antarctic icebergs reorganize ocean circulation during Pleistocene glacials. *Nature*. 589 (7841), 236-241. doi:10.1038/s41586-020-03094-7

Steiger, R. H. & Jäger, E. (1977), Subcommission on geochronology: Convention on the use of decay constants in geo- and cosmochronology. *Earth and Planetary Science Letters*. 36 (3), 359-362. doi:10.1016/0012-821x(77)90060-7

Tanaka, T., Togashi, S., Kamioka, H., Amakawa, H., Kagami, H., Hamamoto, T., Yuhara, M., Orihashi, Y., Yoneda, S., Shimizu, H., Kunimaru, T., Takahashi, K., Yanagi, T., Nakano, T., Fujimaki, H., Shinjo, R., Asahara, Y., Tanimizu, M. & Dragusanu, C. (2000), JNdi-1: a neodymium isotopic reference in consistency with LaJolla neodymium. *Chemical Geology*. 168 (3-4), 279-281. doi:10.1016/S0009-2541(00)00198-4

Tang, Z., Shi, X. F., Zhang, X., Chen, Z. H., Chen, M. T., Wang, X. Q., Wang, H. Z., Liu, H. L., Lohmann, G., Li, P. Y., Ge, S. L. & Huang, Y. H. (2016), Deglacial biogenic opal peaks revealing enhanced Southern Ocean upwelling during the last 513 ka. *Quaternary International*. 425, 445-452.

1100 doi:10.1016/j.quaint.2016.09.020
1101 team, I. (2018), Mass balance of the Antarctic Ice Sheet from 1992 to 2017. *Nature*.
1102 558 (7709), 219-222. doi:10.1038/s41586-018-0179-y
1103 Teitler, L., Warnke, D. A., Venz, K. A., Hodell, D. A., Becquey, S., Gersonde, R. &
1104 Teitler, W. (2010), Determination of Antarctic Ice Sheet stability over the last
1105 ~500 ka through a study of iceberg-rafted debris. *Paleoceanography*. 25
1106 (1)doi:10.1029/2008pa001691
1107 Thoma, M., Jenkins, A., Holland, D. & Jacobs, S. (2008), Modelling Circumpolar
1108 Deep Water intrusions on the Amundsen Sea continental shelf, Antarctica.
1109 *Geophysical Research Letters*. 35 (18)doi:10.1029/2008gl034939
1110 Tigchelaar, M., Timmermann, A., Pollard, D., Friedrich, T. & Heinemann, M. (2018),
1111 Local insolation changes enhance Antarctic interglacials: Insights from an
1112 800,000-year ice sheet simulation with transient climate forcing. *Earth and*
1113 *Planetary Science Letters*. 495, 69-78. doi:10.1016/j.epsl.2018.05.004
1114 Tinto, K. J., Padman, L., Siddoway, C. S., Springer, S. R., Fricker, H. A., Das, I.,
1115 Tontini, F. C., Porter, D. F., Frearson, N. P., Howard, S. L., Siegfried, M. R.,
1116 Mosbeux, C., Becker, M. K., Bertinato, C., Boghosian, A., Brady, N., Burton,
1117 B. L., Chu, W., Cordero, S. I., Dhakal, T., Dong, L., Gustafson, C. D.,
1118 Keeshin, S., Locke, C., Lockett, A., O'Brien, G., Spergel, J. J., Starke, S. E.,
1119 Tankersley, M., Wearing, M. G. & Bell, R. E. (2019), Ross Ice Shelf response
1120 to climate driven by the tectonic imprint on seafloor bathymetry. *Nature*
1121 *Geoscience*. 12 (6), 441-+. doi:10.1038/s41561-019-0370-2
1122 Toggweiler, J. R., Russell, J. L. & Carson, S. R. (2006), Midlatitude westerlies,
1123 atmospheric CO_2, and climate change during the ice ages. *Paleoceanography*.
1124 21 (2), n/a-n/a. doi:10.1029/2005pa001154
1125 Tournadre, J., Bouhier, N., Girard−Ardhuin, F. & Rémy, F. (2016), Antarctic icebergs
1126 distributions 1992–2014. *Journal of Geophysical Research: Oceans*. 121 (1),
1127 327-349. doi:10.1002/2015jc011178
1128 Turner, J., Phillips, T., Hosking, J. S., Marshall, G. J. & Orr, A. (2013), The
1129 Amundsen Sea low. *International Journal of Climatology*. 33 (7), 1818-1829.
1130 doi:10.1002/joc.3558
1131 Turney, C. S. M., Fogwill, C. J., Golledge, N. R., McKay, N. P., van Sebille, E., Jones,
1132 R. T., Etheridge, D., Rubino, M., Thornton, D. P., Davies, S. M., Ramsey, C.
1133 B., Thomas, Z. A., Bird, M. I., Munksgaard, N. C., Kohno, M., Woodward, J.,
1134 Winter, K., Weyrich, L. S., Rootes, C. M., Millman, H., Albert, P. G., Rivera,
1135 A., van Ommen, T., Curran, M., Moy, A., Rahmstorf, S., Kawamura, K.,
1136 Hillenbrand, C. D., Weber, M. E., Manning, C. J., Young, J. & Cooper, A.
1137 (2020), Early Last Interglacial ocean warming drove substantial ice mass loss
1138 from Antarctica. *Proc Natl Acad Sci U S A*. 117 (8), 3996-4006.
1139 doi:10.1073/pnas.1902469117
1140 Ullermann, J., Lamy, F., Ninnemann, U., Lembke−Jene, L., Gersonde, R. &
1141 Tiedemann, R. (2016), Pacific−Atlantic Circumpolar Deep Water coupling
1142 during the last 500 ka. *Paleoceanography*. 31 (6), 639-650.
1143 doi:10.1002/2016pa002932

1144 Wadham, J. L., Hawkings, J. R., Tarasov, L., Gregoire, L. J., Spencer, R. G. M.,
1145 Gutjahr, M., Ridgwell, A. & Kohfeld, K. E. (2019), Ice sheets matter for the
1146 global carbon cycle. *Nature Communications*. 10 (1), 3567.
1147 doi:10.1038/s41467-019-11394-4
1148 Walker, D. P., Brandon, M. A., Jenkins, A., Allen, J. T., Dowdeswell, J. A. & Evans, J.
1149 (2007), Oceanic heat transport onto the Amundsen Sea shelf through a
1150 submarine glacial trough. *Geophysical Research Letters*. 34
1151 (2)doi:10.1029/2006gl028154
1152 Wan, S., Li, A., Clift, P. D. & Jiang, H. (2006), Development of the East Asian
1153 summer monsoon: Evidence from the sediment record in the South China Sea
1154 since 8.5 Ma. *Palaeogeography, Palaeoclimatology, Palaeoecology*. 241 (1),
1155 139-159. doi:10.1016/j.palaeo.2006.06.013
1156 Wan, S. M., Clift, P. D., Zhao, D. B., Hovius, N., Munhoven, G., France-Lanord, C.,
1157 Wang, Y. X., Xiong, Z. F., Huang, J., Yu, Z. J., Zhang, J., Ma, W. T., Zhang, G.
1158 L., Li, A. C. & Li, T. G. (2017), Enhanced silicate weathering of tropical shelf
1159 sediments exposed during glacial lowstands: A sink for atmospheric CO_2.
1160 *Geochimica Et Cosmochimica Acta*. 200, 123-144.
1161 doi:10.1016/j.gca.2016.12.010
1162 Wan, S. M., Tian, J., Steinke, S., Li, A. C. & Li, T. G. (2010), Evolution and
1163 variability of the East Asian summer monsoon during the Pliocene: Evidence
1164 from clay mineral records of the South China Sea. *Palaeogeography*
1165 *Palaeoclimatology Palaeoecology*. 293 (1-2), 237-247.
1166 doi:10.1016/j.palaeo.2010.05.025
1167 Wang, S., Liu, J., Cheng, X., Kerzenmacher, T. & Braesicke, P. (2020), Is Enhanced
1168 Predictability of the Amundsen Sea Low in Subseasonal to Seasonal Hindcasts
1169 Linked to Stratosphere−Troposphere Coupling? *Geophysical Research Letters*.
1170 47 (18)doi:10.1029/2020gl089700
1171 Watkins, N. D., Keany, J., Ledbetter, M. T. & Huang, T. C. (1974), Antarctic glacial
1172 history from analyses of ice-rafted deposits in marine sediments: new model
1173 and initial tests. *Science*. 186 (4163), 533-6. doi:10.1126/science.186.4163.533
1174 Weber, M. E., Clark, P. U., Kuhn, G., Timmermann, A., Sprenk, D., Gladstone, R.,
1175 Zhang, X., Lohmann, G., Menviel, L., Chikamoto, M. O., Friedrich, T. &
1176 Ohlwein, C. (2014), Millennial-scale variability in Antarctic ice-sheet
1177 discharge during the last deglaciation. *Nature*. 510 (7503), 134-8. doi:10.1038/
1178 nature13397
1179 Weber, M. E., Kuhn, G., Sprenk, D., Rolf, C., Ohlwein, C. & Ricken, W. (2012), Dust
1180 transport from Patagonia to Antarctica – A new stratigraphic approach from
1181 the Scotia Sea and its implications for the last glacial cycle. *Quaternary*
1182 *Science Reviews*. 36, 177-188. doi:10.1016/j.quascirev.2012.01.016
1183 Wever, H. E., Millar, I. L. & Pankhurst, R. J. (1994), Geochronology and radiogenic
1184 isotope geology of Mesozoic rocks from eastern Palmer Land, Antarctic
1185 Peninsula: crustal anatexis in arc-related granitoid genesis. *Journal of South*
1186 *American Earth Sciences*. 7 (1), 69-83. doi:10.1016/0895-9811(94)90035-3
1187 Wever, H. E. & Storey, B. C. (1992), Bimodal magmatism in northeast Palmer Land,

1188 Antarctic Peninsula: Geochemical evidence for a Jurassic ensialic back-arc
1189 basin. *Tectonophysics*. 205 (1-3), 239-259. doi:10.1016/0040-1951(92)90429-
1190 a
1191 Wolff, E. W., Barbante, C., Becagli, S., Bigler, M., Boutron, C. F., Castellano, E., de
1192 Angelis, M., Federer, U., Fischer, H., Fundel, F., Hansson, M., Hutterli, M.,
1193 Jonsell, U., Karlin, T., Kaufmann, P., Lambert, F., Littot, G. C., Mulvaney, R.,
1194 Rothlisberger, R., Ruth, U., Severi, M., Siggaard-Andersen, M. L., Sime, L.
1195 C., Steffensen, J. P., Stocker, T. F., Traversi, R., Twarloh, B., Udisti, R.,
1196 Wagenbach, D. & Wegner, A. (2010), Changes in environment over the last
1197 800,000 years from chemical analysis of the EPICA Dome C ice core.
1198 *Quaternary Science Reviews*. 29 (1-2), 285-295.
1199 doi:10.1016/j.quascirev.2009.06.013
1200 Wu, L., Wang, R. J., Xiao, W. S., Ge, S. L., Chen, Z. H. & Krijgsman, W. (2017),
1201 Productivity-climate coupling recorded in Pleistocene sediments off Prydz
1202 Bay (East Antarctica). *Palaeogeography Palaeoclimatology Palaeoecology*.
1203 485, 260-270. doi:10.1016/j.palaeo.2017.06.018
1204 Wu, L., Wilson, D. J., Wang, R., Passchier, S., Krijgsman, W., Yu, X., Wen, T., Xiao,
1205 W. & Liu, Z. (2021), Late Quaternary dynamics of the Lambert Glacier-
1206 Amery Ice Shelf system, East Antarctica. *Quaternary Science Reviews*. 252
1207 doi:10.1016/j.quascirev.2020.106738
1208 Ziegler, M., Diz, P., Hall, I. R. & Zahn, R. (2013), Millennial-scale changes in
1209 atmospheric CO2 levels linked to the Southern Ocean carbon isotope gradient
1210 and dust flux. *Nature Geoscience*. 6 (6), 457-461. doi:10.1038/ngeo1782